

pubs.acs.org/JACS Article

Molecular Routes of Dynamic Autocatalysis for Methanol-to-Hydrocarbons Reaction

Shanfan Lin, Yuchun Zhi, Wei Chen, Huan Li, Wenna Zhang, Caiyi Lou, Xinqiang Wu, Shu Zeng, Shutao Xu, Jianping Xiao,* Anmin Zheng,* Yingxu Wei,* and Zhongmin Liu*



Cite This: J. Am. Chem. Soc. 2021, 143, 12038–12052



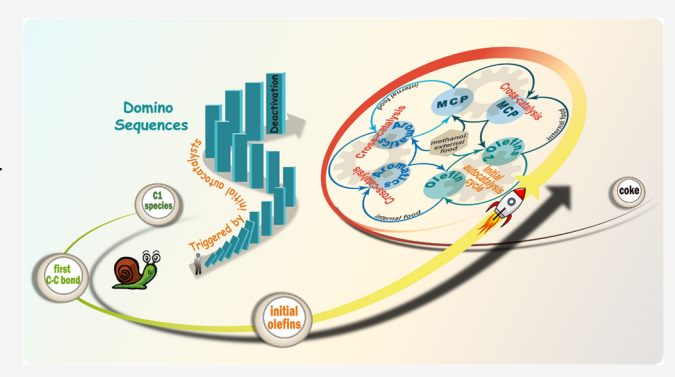
ACCESS

III Metrics & More



s Supporting Information

ABSTRACT: The industrially important methanol-to-hydrocarbons (MTH) reaction is driven and sustained by autocatalysis in a dynamic and complex manner. Hitherto, the entire molecular routes and chemical nature of the autocatalytic network have not been well understood. Herein, with a multitechnique approach and multiscale analysis, we have obtained a full theoretical picture of the domino cascade of autocatalytic reaction network taking place on HZSM-5 zeolite. The autocatalytic reaction is demonstrated to be plausibly initiated by reacting dimethyl ether (DME) with the surface methoxy species (SMS) to generate the initial olefins, as evidenced by combining the kinetic analysis, *in situ* DRIFT spectroscopy, 2D ¹³C-¹³C MAS NMR, electronic states, and projected density of state (PDOS) analysis. This process is



operando tracked and visualized at the picosecond time scale by advanced ab initio molecular dynamics (AIMD) simulations. The initial olefins ignite autocatalysis by building the first autocatalytic cycle—olefins-based cycle—followed by the speciation of methylcyclopentenyl (MCP) and aromatic cyclic active species. In doing so, the active sites accomplish the dynamic evolution from proton acid sites to supramolecular active centers that are experimentally identified with an ever-evolving and fluid feature. The olefins-guided and cyclic-species-guided catalytic cycles are interdependently linked to forge a previously unidentified hypercycle, being composed of one "selfish" autocatalytic cycle (i.e., olefins-based cycle with lighter olefins as autocatalysts for catalyzing the formation of olefins) and three cross-catalysis cycles (with olefinic, MCP, and aromatic species as autocatalysts for catalyzing each other's formation). The unraveled dynamic autocatalytic cycles/network would facilitate the catalyst design and process control for MTH technology.

INTRODUCTION

Catalysis, a key pillar of modern industry, brings about the conspicuous rate acceleration of a reaction by the catalyst. Autocatalysis, a particular case of catalysis, refers to a process in which a reaction product acts as the catalyst, exponentially accelerating the reaction by producing more of itself. As a self-sustained process, autocatalysis has fascinated scientists for centuries from across biology system, materials science, chemistry, and so on. While being ubiquitous and extensively studied in biosystems and materials science, autocatalysis is rare and less studied in the zeolite catalysis field.

In zeolite catalysis chemistry, both autocatalysis and nanoconfinement can appreciably accelerate chemical reaction. Autocatalysis represents the guest (product)-mediated accelerated chemical reaction. The classic autocatalytic reactions, such as ester hydrolysis⁵ and formose reaction,⁶ were carried out in organic solvent or open space, not in confined space, invoking the product selectivity out of control. Nanospace confinement reflects the host-mediated accelerated chemical reaction—which is induced by molecular-sized confines

(nanoenvironments) of the host—prevalent in, e.g., enzyme catalysis⁷ and zeolite catalysis.⁸ In confined space, catalytically active sites synergizing with its microenvironments aid in enriching, activating substrates, and stabilizing the reaction transition state, via individually weak but collectively strong noncovalent interactions.⁹ However, less is known about the autocatalysis in zeolite confined space. The industrially relevant methanol-to-hydrocarbons (MTH) reaction can serve as an exceptional probe: it combines, in essence, autocatalysis and nanoconfinement in one.

The MTH process over zeolite and zeotype catalysts has become the most successful nonpetroleum route for producing light olefins and gasoline. Despite the industrial success of this

Received: April 1, 2021 Published: July 28, 2021





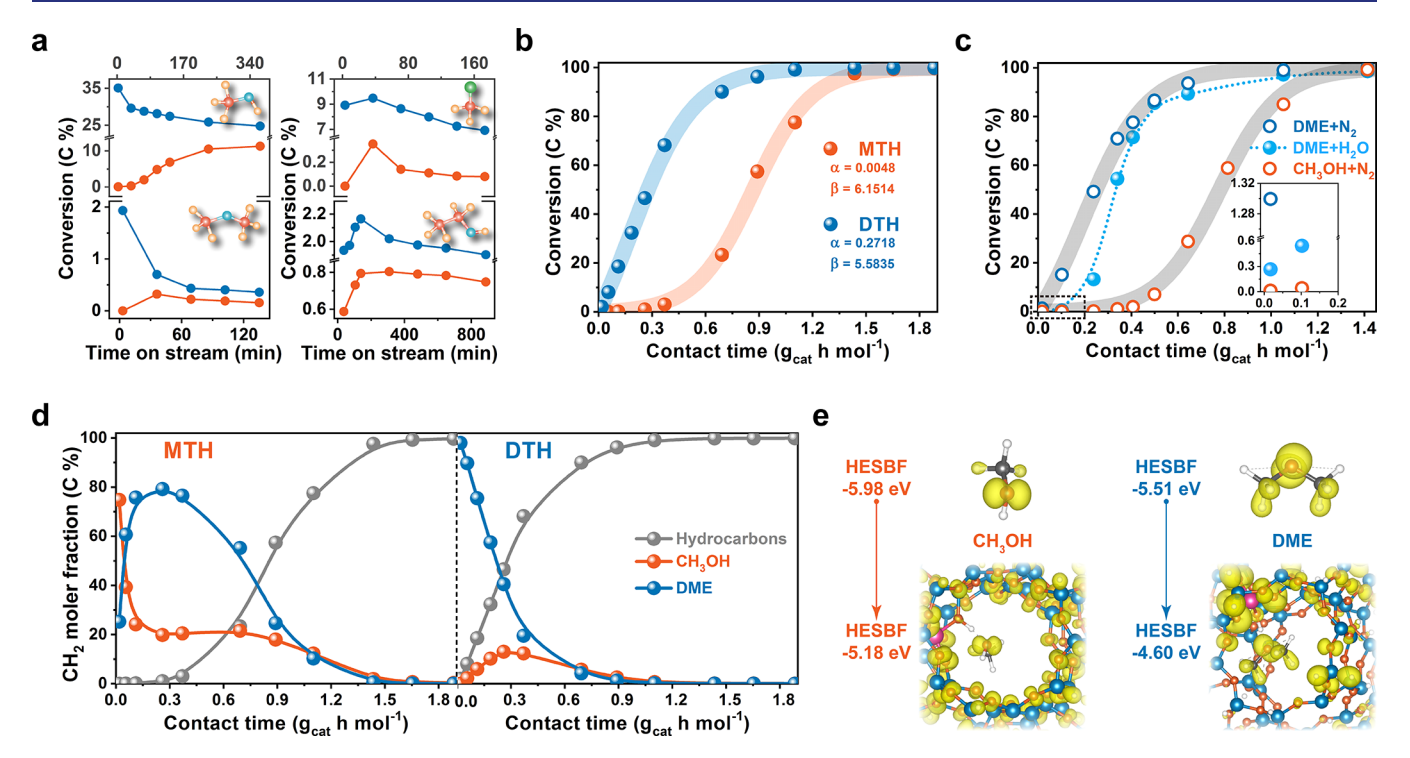


Figure 1. Autocatalysis performance and kinetic feature. (a) Time-dependent autocatalytic curves (orange) for methanol, DME, CH₃Cl, and ethanol, as well as with cofed propene (blue), conducted over HZSM-5-90 (Si/Al = 90) at 578, 443, 463, and 540 K, respectively, with equimolar carbon feeding (0.0062 mol h⁻¹). The ratio of molar carbon of each reactant to propene was approximately 104:9. (b) Conversions of methanol and DME against contact time after 170 s reaction over HZSM-5-90 at 623 K, with product distributions shown in Figure S5. Points, experimental results; solid lines, fitted lines according to eq 3. (c) Effect of conversion-specific coadded water on DME conversion over HZSM-5-90 at 623 K. (d) Effluent compositions of methanol and DME with contact time, corresponding to the experiments in Figure 1b. (e) Energies of HESBF for methanol and DME in gas phase and in zeolite confined space, where the isosurface levels of partial charge density were set as 0.03 and 0.01 for methanol and DME, respectively.

process, the upgrading of current industry technology necessitates a systematic and thorough mechanistic understanding. Control of product selectivity is a long-standing pursuit of MTH chemistry and industry; comprehensive interpretation of the autocatalytic mechanism and complex reaction network are the prerequisites to realize this goal.

The MTH reaction over zeolite was discovered by Chang in 1977. 10 Soon, the autocatalytic character of the MTH reaction was disclosed by Chen and Reagan via reprocessing of Chang's original results.¹¹ Later, olefins were suggested by Dessau and LaPierre as autocatalytic species and an olefin methylationcracking mechanism was considered as the main reaction pathway on HZSM-5, 12,13 whereas aromatic species were treated as products and coke precursors.¹⁴ Nevertheless, the importance of cyclic species such as aromatics in the MTH reaction was evidenced by experiments of cofeeding small amounts of toluene or p-xylene, which significantly accelerated the methanol conversion. ^{15,16} On the basis of these results, the aromatic cocatalysis effect was proposed. ^{15,16} In the 1990s, Dahl and Kolboe proposed the hydrocarbon pool concept based on the low reactivity of olefins when cofed with methanol over SAPO-34,¹⁷⁻¹⁹ while chemical identity of the pool species (CH₂), adsorbed on zeolite surface was not specified. Later, polymethylbenzenes and their protonated counterparts were successfully captured and identified as the dominant hydrocarbon pool species over SAPO-34.20-22 Similar findings were reported for large-pore zeolites such as H-BEA and H-MOR.^{23–25} In these contexts, the dual-cycle mechanism, with olefins-based and aromatics-based cycles operating simultaneously during the MTH reaction over

HZSM-5 was proposed by Olsbye, $^{26-28}$ with ethene (and propene 29) being mainly formed from the lower methylbenzenes by an aromatics-based cycle and C_3^+ olefins formed from an olefins-based cycle. The olefins- and aromatics-based cycles are interdependently interactive, constituting the pseudo-steady-state reaction network, functioning as a catalytic scaffold to drive methanol conversion. Recently, a methyl-cyclopentenyl (MCP)-based cycle (which bridges the traditional dual cycles) was supplemented, making the reaction network more complex and cooperative. 30

The development of MTH chemistry over the past 40 years has greatly extended our knowledge on the basic principle of methanol conversion. The autocatalysis-driven complex reaction network has been recognized but not unambiguously demonstrated. 31,32 To uncover the autocatalytic motif in zeolite confined space, it is imperative to map, in greater detail, the structural and chemical information on real active sites, confined molecular species, and their complex interactions. To arrive at the dynamic nature and a fullspectrum autocatalytic mechanism of the MTH reaction, the following crucial issues should be resolved: What is the chemical origin of the induction period of methanol conversion? How are the autocatalytic cycles built? What is the chemical nature of the autocatalytic reaction network? The challenge lies in dynamic, complex, and diverse autocatalytic patterns: the chemical identities and fates of surface species diverge largely; the ever-evolving active centers associated with the dynamic host-guest interactions induce additional chemical complexity; the diverse and interactive elementary events complicate the reaction network. The intricacy of the

autocatalytic mechanism necessitates the integration of multiple analytical techniques, rather than depending on any single one.

In this work, we build a multitechnique approach (by integrating kinetics, electronic states analysis, projected density of state (PDOS) electronic interaction analysis with ab initio molecular dynamics (AIMD) simulations, and multiple in situ and operando spectroscopic analyses), which enables multiscale analysis (across nanosized microenvironment to molecule and electron scale; from second to picosecond time scale). With this, we delineate how autocatalysis is initiated, sustained, and decaying in an industrially important, zeolite-catalyzed MTH as a model reaction. Full-spectrum molecular routes of a domino cascade of a reaction network are mapped. We in situ and operando monitor the building courses of different kinds of autocatalysts and their leading autocatalytic cycles. By doing so, we uncover the chemical genesis of the induction period of autocatalysis. The chemical nature of autocatalytic cycles has been refined and described as a hypercycle with one "selfish" autocatalytic cycle and three cross-catalysis cycles.

■ RESULTS AND DISCUSSION

General Feature and Kinetic Signature of Autocatalysis. The conversions of C1 species (methanol, DME, and CH₃Cl) and ethanol on HZSM-5-90 (see physicochemical properties in Figures S1–S3 and Table S1) against reaction time showed a sigmoidal kinetic profile: the reactions were initially slow during the induction stage as little autocatalysts were present and they were progressively accelerated with the formation of more autocatalysts (Figure 1a). The observed S-shaped curve is, however, insufficient to validate the existence of authentic autocatalysis, because both the activation of a precatalyst and product self-induction can also lead to a sigmoidal profile.³³ Yet, cofeeding of propene with C1 species and ethanol remarkably shortened or eliminated the induction period (Figure 1a), corroborating that these reactions are of autocatalytic nature, with propene as one kind of autocatalyst.

Next, we used the MTH reaction as a probe, aiming to build a full molecular picture of autocatalytic mechanism. The DME-to-hydrocarbons (DTH) reaction was taken as a reference given the following considerations: (1) the traditionally viewed thermodynamic equilibrium of CH₃OH–DME interconversion was actually broken during the MTH process (see Figure S4), in line with a previous report; ³⁴ (2) surface reagent pools inside zeolite pores are rather diverse and complex and, in view of this, taking sole DME as the reactant would simplify the reaction system.

The autocatalytic profiles of contact-time-dependent MTH and DTH reactions performed over HZSM-5-90 at 623 K differed apparently (Figure 1b). The sigmoidal MTH profile exhibited a kinetically sluggish induction period, followed by a rapid ascending period, during which substantial autocatalysts were progressively generated, enabling exponential propagation of autocatalytic turnover. In stark contrast, the DTH profile showed a linear and very quick growth from onset of reaction, indicative of the remarkable reactivity of the DTH reaction. To ensure this observation was not a coincidence, we tested the DTH reaction at various temperatures such as 573 and 523 K, and as expected, the incipient linear scaling still held (Figure S6). This surprisingly high reactivity of the DTH reaction (where DME was traditionally treated as a similar C1 species with methanol³⁵) was verified by the temperature-programmed surface reaction (TPSR) and time-dependent temperaturevarying experiments (Figures S7 and S8). To eliminate the possible effect from catalytically environmental discrepancy, "pre-activated" catalysts with "seeds" grown by methanol or DME pre-reaction were created. The following DTH reaction on such catalysts with identical working environments dramatically outperformed the MTH reaction, further supporting the preceding conclusions (Figure S9).

To achieve quantitative kinetic analysis, a simplified autocatalytic reaction scheme was expressed as follows:³⁶

$$R + R \xrightarrow{k_1} P \tag{1}$$

$$R + P \xrightarrow{k_2} 2P \tag{2}$$

where R is reactant; P is hydrocarbon product; k_1 and k_2 represent the rate constants of direct coupling of two C1 species and the following autocatalytic reaction, respectively.

The autocatalytic kinetic model was derived as (see the Supporting Information for derivations)

$$x = 1 - \frac{1}{1 + \alpha[\exp(\beta \tau) - 1]}$$
 (3)

where x is the conversion of the reactant and τ is the contact time $(W_{\text{cat.}}/F_{[R]_0})$, with $[R]_0$ as the incipient concentration of the reactant. Two kinetic parameters, α and β , are defined: $\alpha = k_1/k_2$ and $\beta = k_2[R]_0$. The variations in α and β produced various S-shaped patterns of autocatalytic curves (Figure S10).

We fitted the experimental data in Figure 1b with eq 3 to quantitatively yield kinetic information. The comparable values of k_2 , deduced from the comparable β values (6.1514 and 5.5835 for MTH and DTH reactions, respectively), suggest the similar reactivities of methanol and DME during the highly efficient autocatalytic stage. For the MTH reaction, the calculated value of α is 0.0048, signifying the much lower value of k_1 than k_2 , corresponding to the sluggish kinetics to initiate autocatalysis. While for the DTH reaction, α is 0.2718, \sim 57 times higher than that of the MTH reaction, meaning significantly accelerated kinetics to initiate autocatalysis, in view of the comparable k_2 .

Ruling Out Product Water Effect. We wonder if such prominent incipient reactivity differences are derived from the product water effect, given methanol and DME conversion differences and the concomitant water amount differences diverging largely with contact time (Figure 1b). To address this question, we carefully designed DME-water cofeeding experiments, with the added water amount being respectively estimated under each contact time (see Table S2 for details). Upon separately adding the corresponding amount of water, DME conversions were mainly maintained, except for the slight decrease at short contact times (Figure 1c). Adopting the traditional water cofeeding mode, however, gave a quite different picture: with DME to water ratios of 1:0.1 and 1:0.25, DME conversions slightly decreased; but with increasing the ratio to 1:1, DME reactivity was apparently depressed (Figure S11). This, in turn, validated the rationality and necessity of the preceding conversion-specific water addition scenario.

Analysis of these experimental results, together with the calculated 106 and 30 kJ/mol higher proton affinity and adsorption enthalpy of DME than those of water (Figure S12 and Table S3), allows us to argue that the competitive adsorption between DME and water may exist, but to what extent depends on the relative water contents and reaction conditions. The exceptional incipient reactivity of DTH

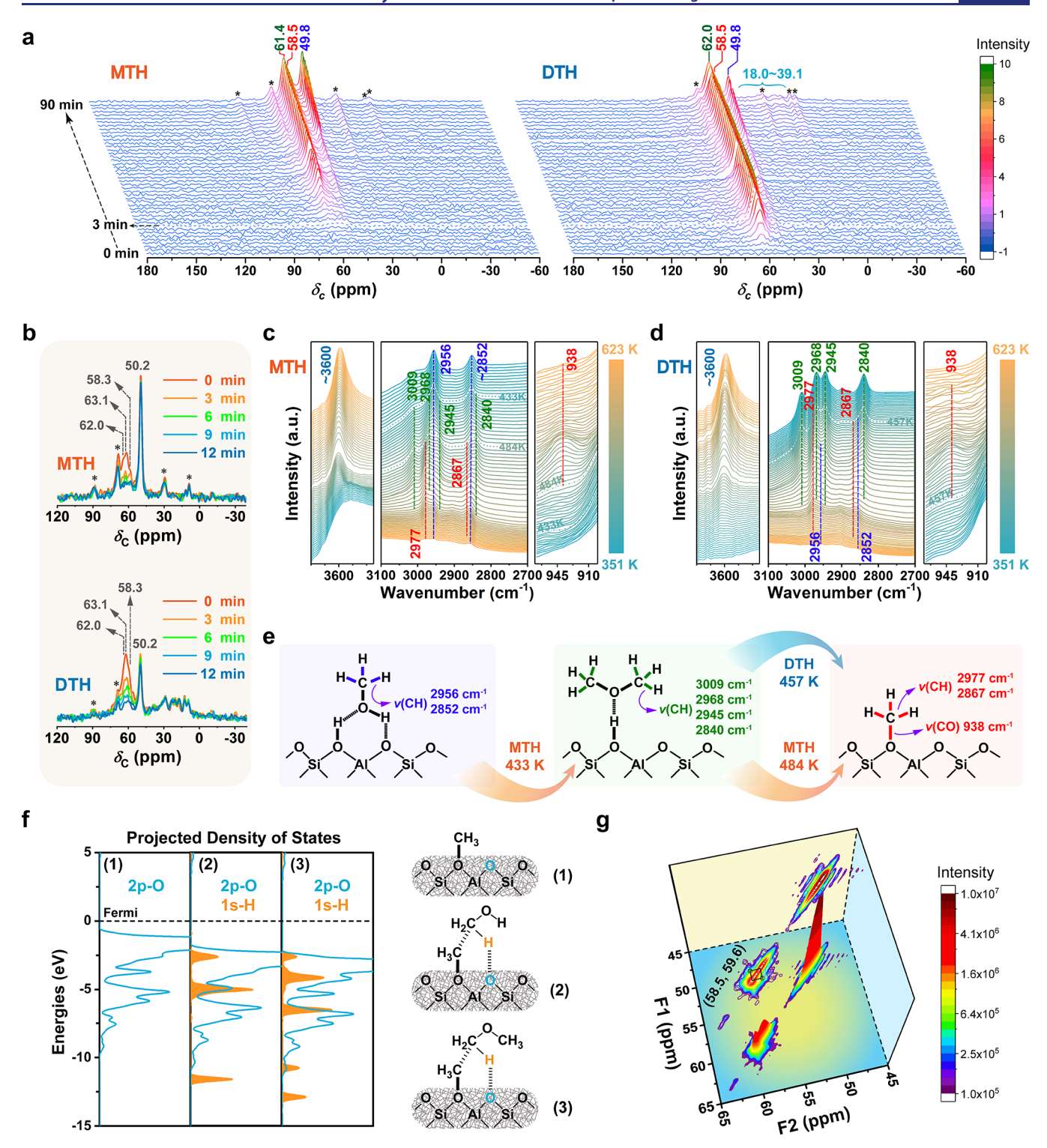


Figure 2. Multimodal monitoring of surface species and microenvironments. (a, b) *In situ* solid-state ¹³C MAS NMR spectra recorded during ¹³C-methanol and ¹³C-DME conversion on HZSM-5-90 at 573 K for 0–90 min (a), and then the reactant flow was switched to helium flow for 0–12 min (b). Asterisk (*) indicates the spinning sideband. (c, d) *In situ* TPD-DRIFT spectra recorded during methanol and DME TPD experiments on HZSM-5-15 (Si/Al = 15). (e) Characteristic vibrational bands of adsorbed methanol, DME, and the SMS, with detailed assignments shown in Figure S13. (f) Projected density of state analysis for interactions of methanol and DME with the SMS via monitoring electronic energy changes of the methyl H of methanol or DME and framework O of HZSM-5 zeolite. Fermi level is shifted to 0 eV. (g) 2D ¹³C – ¹³C CORD (combined R2ⁿ_ν-driven) spin diffusion MAS NMR correlation spectra for C1 species on HZSM-5-90 after MTH reaction for 20 s at 573 K, with a mixing time of 200 ms.

relative to the MTH reaction is not caused by *in situ* produced water, but it may be related to the intricate surface molecular behavior and local microenvironments.

From Ensemble Kinetic Behavior to Molecular Details. The foregoing kinetic analyses revealed the ensemble behavior of an autocatalytic reaction. Next, we will analyze the

detailed molecular behavior to illuminate the incipient reactivity and induction of autocatalysis.

We first identified DME as a more reactive C1 species in constructing the initial C–C bond containing species. Within the incipient stage of the MTH reaction, the DME concentration appeared to have a sharp increase, accompanied by a jump decrease of the methanol concentration (Figure 1d). After it reached the highest concentration, DME gradually decreased. In parallel with the decrease of DME, hydrocarbons started to appear and then exponentially ascended, which was the same as that for the DTH reaction. These observations allow the deduction that autocatalytic reaction sets in only after a substantial concentration of DME has been accumulated.

This deduction was later theoretically supported by energy analyses of the highest electronic states below Fermi level (HESBF). Note that the energy analyses of the frontier molecular orbitals (HOMO and LUMO) are widely used in molecular systems. However, it is not proper to use HOMO/ LUMO to describe the delocalized nature of adsorbates on solid catalysts. In order to describe the difference in electronic structures of reactants between gas phase and zeolite confined space, we analyzed the HESBF, which is similar to the HOMO. The constrained environments of zeolite can exert an electron confinement effect on the confined molecules via increasing the energies of the frontier molecular orbitals. 37,38 The increase of HOMO energies tends to be more prominent than that of LUMO energies, and the higher HOMO energies signify the increased basicity of the confined molecules.³⁸ Analogously, zeolite confined space would increase the energies of electronic states of the confined molecules. The energies of the HESBF increased by 0.8 and 0.91 eV, respectively, for methanol and DME in the HZSM-5 channel relative to in gas phase (Figure 1e), suggesting a marked pre-activation of DME compared with methanol in zeolite confined space.

Surface Species and Microenvironment Effect on Induction of Autocatalysis. Having delineated the molecular details of critical effluent species, we now turn to monitor, by *in situ* spectroscopic approaches, the surface adsorbed species, local microenvironments, and their effect on induction of autocatalysis.

In situ ¹³C MAS NMR was adopted to track the surface adsorbed species by continuously feeding ¹³C-methanol or ¹³C-DME into the rotor reactor at 573 K (Figure 2a). A timeresolved array of NMR spectra showed that, at incipient DTH reaction, surface adsorbed C1 species appeared in sequence: DME (62 ppm)^{39–41} at 60 s, the SMS (58.5 ppm)^{39–41} at 80 s, and methanol (49.8 ppm)^{39–41} with a weak signal at 120 s. While for the MTH reaction, the appearance of these surface C1 species was largely delayed and occurred after reaction for 3 min. In situ NMR results reflect the relatively sluggish kinetics of methanol to construct surface active C1 intermediates.

After *in situ* reaction for 90 min, the feeds of methanol or DME were stopped and the catalysts were swept with helium to collect the NMR spectra. Surprisingly, both for MTH and DTH reactions, DME (62 and 63.1 ppm) and the SMS (58.3 ppm) signals declined rapidly, but methanol signals (50.2 ppm) remained almost unchanged (Figure 2b). The similar phenomenon was also observed by temperature-programmed desorption (TPD) diffuse reflectance infrared Fourier transform spectroscopy (DRIFT) experiments (Figure S14). These spectroscopic observations implicate DME and the SMS as two more reactive C1 species in the initial reaction stage.

Next, *in situ* TPD–DRIFT experiments were carried out to monitor more detailed surface C1 species evolution (Figure 2c–e). For the MTH reaction, methanol (2956 and 2852 cm⁻¹)^{42,43} first dehydrated to form DME (3009, 2968, 2945, and 2840 cm⁻¹)^{42,43} at 433 K and subsequently to form the SMS (2977, 2867, and 938 cm⁻¹)^{42–44} at 484 K (Figure 2c). The appearance sequence of these C1 species implied that the SMS was more readily originated from DME than from methanol. This finding accords with previous *in situ* IR results, ⁴³ and it is energetically favored by the lower Gibbs free energy barrier of 26.8 kcal/mol for DME to the SMS (via trimethyloxonium intermediate) than that of 33.3 kcal/mol for methanol directly decomposing to the SMS.⁴⁵

Notably, for the DTH reaction, DME decomposed to form the SMS at 457 K (Figure 2d), a temperature much lower than 484 K for DME to the SMS in the MTH reaction (Figure 2c). The reason may lie in the presence of the less reactive surface species, such as methanol dimer or cluster, during the MTH reaction, as inferred from a kinetic proof of alcohol dimer during zeolite catalysis, ⁴⁶ and as evidenced by *in situ* TPSR–DRIFT experiments confirming the appearance of methanol cluster (centered at 3300 cm⁻¹) ⁴⁷ (Figure S15). However, this would not be the case for the less polar DME. The emergence of these inactive surface species, along with the tendency for methanol to readily form side products of methane and formaldehyde (Figure S16), well explain the rather low incipient reactivity and slow induction of autocatalysis for the MTH reaction (Figure 1b).

Initiation of Autocatalysis. The initiation of autocatalysis needs to activate and react two active C1 species. Analyses from kinetics, HESBF energies, and *in situ* NMR and DRIFT spectroscopies have identified DME as one kind of more reactive C1 species; the reactivity of the SMS has been verified in this and previous work. Consequently, reacting DME with the SMS holds great promise to construct initial C–C bond species that ignite autocatalysis.

This speculation was first theoretically supported by PDOS analysis of the electronic interactions between methanol or DME and the SMS as shown in Figure 2f. The 1s H orbital (methyl H of methanol or DME) overlapped with the 2p O orbital (framework O of ZSM-5 zeolite) in energy, which implied the existence of electronic interactions. The electronic resonance shifted to a deeper state for DME than for methanol, indicating the stronger H-bonding interaction between methyl H and framework O. This, in turn, indicated that the C–H bond of DME was more deeply activated than that of methanol by the SMS. Thus, DME more readily reacted with the adjacent SMS.

Direct evidence for this theoretical proposal stemmed from the powerful 2D 13 C $^{-13}$ C CORD MAS NMR correlation spectroscopy, which probed the spatial proximity and the strong interactions of surface C1 species on HZSM-5-90 after MTH reaction for 20 s at 573 K (Figure 2g). Except for two sets of self-cross-peaks for methanol at 50.2 ppm and for DME at 59.6 ppm, a pair of cross-peaks between DME (59.6 ppm) and the SMS (58.5 ppm) were successfully captured, but the cross-peaks between methanol and the SMS were not detected. The correlations between the surface adsorbed methanol/DME with the SMS on SAPO-34 were also detected in previous work. 44,49 Our 2D 13 C $^{-13}$ C NMR results deliver direct experimental evidence for directly coupling DME with the SMS.

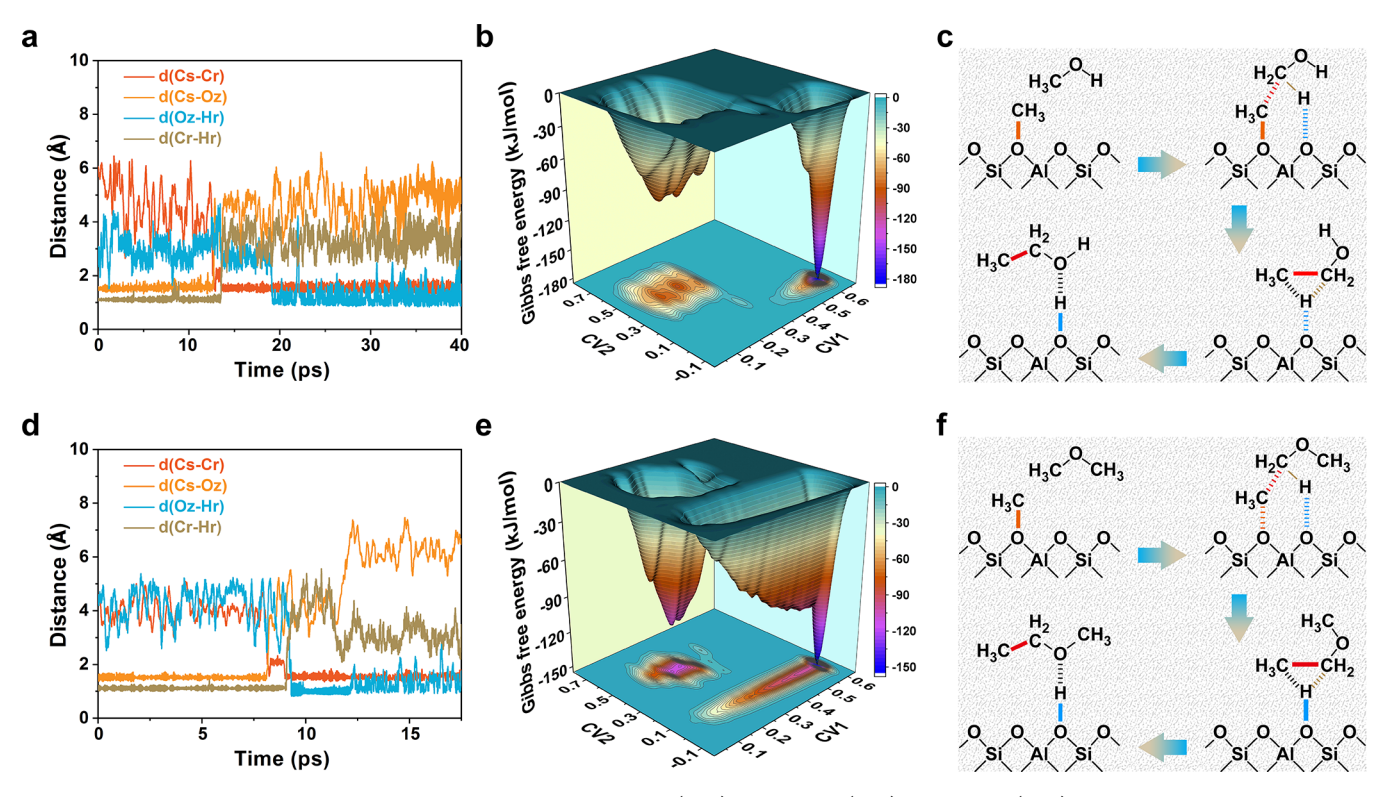


Figure 3. Operando AIMD simulation for SMS-mediated methanol (a–c) and DME (d–f) activation. (a, d) Evolution trajectories of bond distances d(Cs-Oz), d(Cr-Hr), d(Cs-Cr), and d(Oz-Hr), at picosecond time scale, at 673 K over HZSM-5. (b, e) 2D-FES and its projection. Two collective variables (CVs), reflecting the coordination numbers (CNs) on 2D-FES, were adopted to visualize the dynamic process by monitoring the chemical bond formation and cleavage. CV1 = CN(Cs-Oz) describes the breaking of C-O bond of the SMS, and CV2 = CN(Cs-Cr) represents the forming of C-C bond. The atom labels and schematic of the two CVs are shown in Scheme S1. (c, f) Plausible reaction pathways for constructing the initial C-C containing species by the SMS-mediated methanol/DME routes.

The PDOS analysis and 2D ¹³C-¹³C NMR experiment substantiate the proposal of reacting DME with the SMS as a more plausible route to generate the initial C-C species to initiate autocatalysis; however, the mechanistic details are hitherto unclear. By means of AIMD simulations, a powerful tool in computational chemistry, we can *operando* track and visualize the dynamic activation and reaction process of methanol/DME with the SMS at the picosecond time scale (Figure 3).

The chemical bond evolving trajectories, associated with the feasible mechanistic pathways on a two-dimensional free energy surface (2D-FES), provided rich information on the hidden dynamic molecular routes (Figure 3). When methanol or DME approached the SMS, collisions/interactions stretched the Cs-Oz bond of the SMS (Figure 3a,d), marking a transition of the C-O bond from covalent to ionic property. The Cr-Hr bond of methanol/DME was elongated with the assistance of framework oxygen, the activation of which was also implicated by the PDOS analysis for 2p O1 and 1s H orbitals shown in Figure 2f. The Cs-Cr bond formed synchronously by the nucleophilic attack of methanol/DME with the SMS. Cs-Cr bond formation was paralleled with Cr-Hr bond breakage; these processes coincided with (for methanol), or after (for DME), Cs-Oz bond ionization of the SMS. Finally, the proton H (originating from the broken Cr-Hr) returned to framework O to recover zeolite acidity. The detailed molecular pathways for the SMS-mediated methanol/DME routes for constructing the initial C-C containing species are shown in Figure 3c,f. 2D-FES exhibited the minimal energy pathways with two separate low-energy

regions, corresponding to the reactant and product states (Figure 3b,e). The minimal energy pathways on 2D-FES demonstrated that the free energy barrier (154 kJ/mol) for the SMS-mediated DME pathway was lower than that (184 kJ/mol) for the SMS-mediated methanol pathway for generating initial C-C species.

Operando Monitoring of the Whole Autocatalytic Process. Having identified the SMS-mediated DME pathway with high feasibility to initiate autocatalysis, next we will monitor the whole autocatalytic process by the operando approach—combining DRIFT spectra and mass spectroscopy—which provides molecularly specific and time-resolved information on the dynamic evolution of autocatalysis.

Dynamic surface and effluent species profiles with reaction time for methanol and DME conversion are shown in Figure 4a,b and Figure S17. For methanol conversion (Figure 4a), upon adsorption of methanol (2956 and 2852 cm⁻¹),^{42,43} DME (3009, 2968, 2945, and 2840 cm⁻¹)^{42,43} was instantly formed and quickly decomposed to the SMS (2977, 2867, and 938 cm^{-1})⁴²⁻⁴⁴ in the first 1.4 min; soon after, olefinic cations (2963, 2924, and 2870 cm⁻¹)⁵⁰ appeared, concurrent with the online mass spectroscopy observations of their neutral counterparts (Figure S17). Gradually, the SMS diminished and Brønsted acid sites (BAS) were regenerated. The olefins were subject to H-transfer and cyclization reactions with dienes and cycloolefins being experimentally captured as intermediates as shown in Figure S18. Then, the dimethylcyclopentenyl (DMCP) cationic species (3125 and 1510 cm⁻¹)^{50,51} appeared at 6.2 min in the DRIFT spectra for methanol conversion, which were also detected by ¹³C CP/MAS NMR in Figure

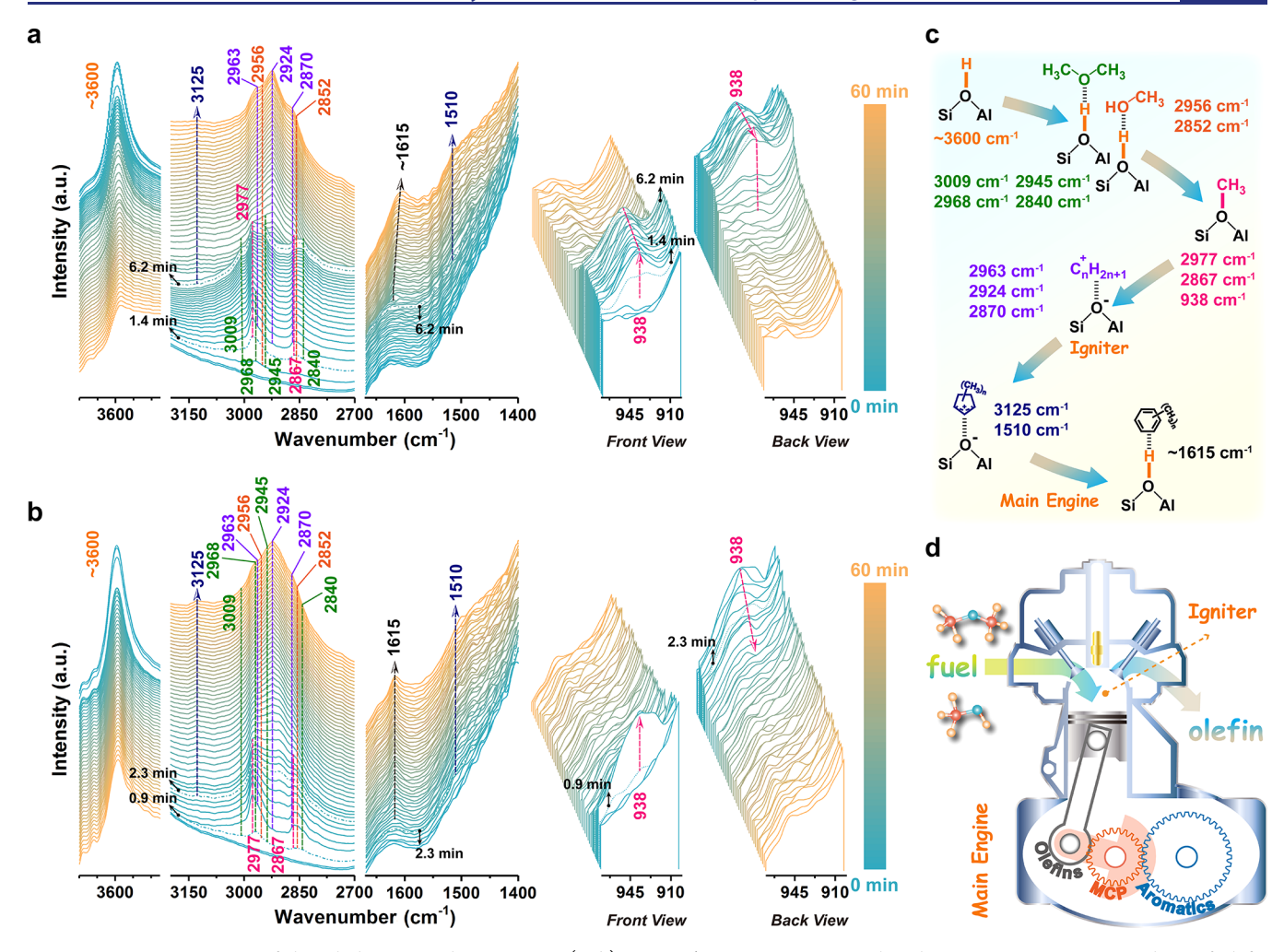


Figure 4. Dynamic routes of the whole autocatalytic process. (a, b) *Operando* DRIFT spectra with online mass spectroscopy analysis of olefin products for tracking the evolution of both surface and effluent species on HZSM-5-15 for methanol conversion (a) and DME conversion (b) at 623 K for 60 min. (c) Dynamic evolving trajectories of surface active species spectroscopically identified. (d) Sketch illustration that compares the methanol/DME conversion process to an automobile engine, with methanol/DME as "fuel" molecules, initial olefin as the "igniter" to initiate autocatalysis, and reactive hydrocarbons as the "main engine" to sustain autocatalysis.

S19, followed by the formation of aromatic species (1615 cm⁻¹).^{44,52} The similar evolving routes were also observed for DME conversion, except that the SMS was quickly built and faded away (Figure 4b).

Real-time DRIFT tracking of zeolite surface species allows us to draw a clear picture of the dynamic evolving routes of the active organics (Figure 4c). The acidic proton catalyzes the formation of DME and the SMS; the SMS reacts with DME (or methanol to a lesser extent) to generate initial olefins; olefinic species, together with the following formed MCP and aromatic species, then relay the SMS as active species to initiate and sustain autocatalysis. In parallel with the directed evolution of active organic species, methanol/DME conversion comes to an indirect reaction stage featuring the exponential rate enhancement of autocatalytic reaction.

The chemically "fueled" autocatalytic process leads us to compare it to an automobile engine. An illustrating demonstration is sketched in Figure 4d. Methanol/DME works as "fuel" molecules to power the autocatalytic system. The autocatalytic reaction is triggered by the initial olefin, and in this sense, the initial olefin can be viewed as the "igniter" of autocatalysis. Lying in the core of the autocatalysis, the reactive hydrocarbons (including olefins, MCP, and aromatic species),

working as accelerants, can be treated as the "main engine" to sustain autocatalysis.

Supramolecular Microenvironment Catalysis. Methanol/DME performs autocatalysis with organic hydrocarbons confined in the zeolite channel as autocatalysts. Herein, we took propene, trimethylbenzene (TriMB), propene-DME complex, and TriMB-DME complex as prototypes, to probe the molecular pre-activation reflected by their HESBF energy increases in the HZSM-5 channel relative to in the gas phase. The electron confinement conferred by the constrained zeolite environments aroused increases of 1.83 and 2.53 eV in the energies of HESBF for propene and TriMB, respectively (Figure 5a). In complex with DME, propene and TriMB show increases of 2.43 and 2.83 eV, respectively, in the HESBF energies. The remarkably increased HESBF (HOMO) energies correspond to an increase in the basicity of the confined molecules that favors electron transfer, 38 which clearly demonstrates the pre-activation of hydrocarbon molecules. Consequently, such pre-activated olefin and aromatics tend easily to perform an electrophilic substitution reaction such as the methylation reaction to propagate autocatalytic chains.

The pre-activation of hydrocarbon molecules in zeolite confined space distinctly reflects the prominent host–guest

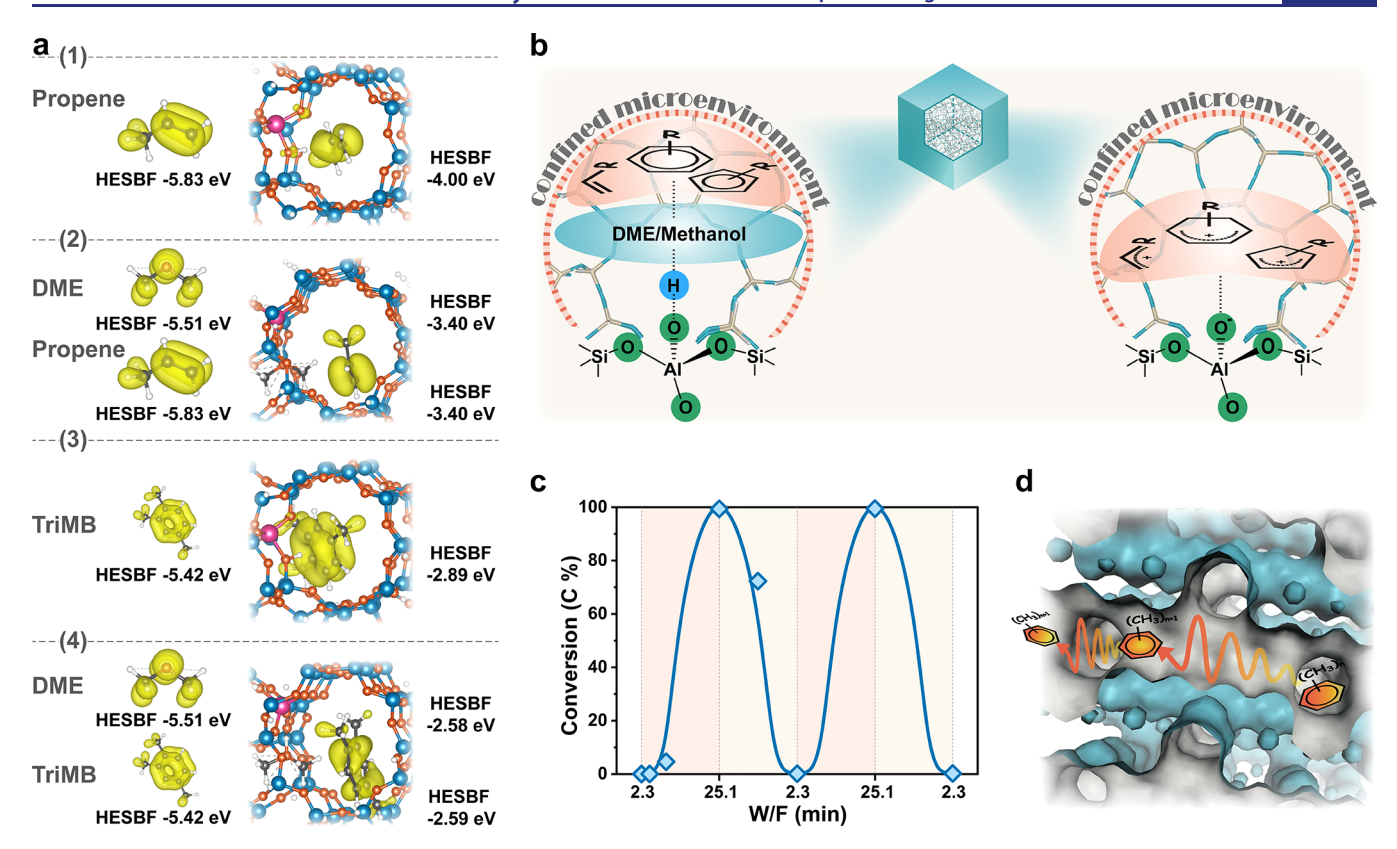


Figure 5. Supramolecular microenvironment active centers and their dynamic behavior. (a) Energies of HESBF for propene, TriMB, and their respective complexes with DME in gas phase and in zeolite confined space, where the isosurface level of partial charge density was set to 0.005. (b) Supramolecular active center by forming the π complex or ion-pair complex during methanol/DME conversion. (c) Methanol conversion with repeated conversion cycles on HZSM-5-90 by periodically adjusting the contact time from 2.3 to 25.1 min (with fixed catalyst amount and variable flow rate) at 623 K. (d) Illustration of the "fluid hydrocarbon pool" concept.

interactions; the underlying spatial interaction/proximity between the accommodated hydrocarbons and the zeolite framework was experimentally evidenced by $^{13}\mathrm{C}-^{27}\mathrm{Al}$ NMR spectroscopy. The confining hydrocarbons laterally associating with methanol/DME interact with BAS to form the π complexes, while the carbocations (the counterpart of neutral hydrocarbons) electrostatically interact with framework O to form the ion-pair complexes (Figure 5b). These organic substances associated with their local zeolite microenvironments constitute the supramolecular active centers, functioning as the true active centers to drive the autocatalysis. We refer to this process as supramolecular microenvironment catalysis.

The following experiments illustrated the dynamic behavior of those in-built supramolecular active centers. By periodically varying the contact time, the catalytic reactivity of methanol was almost entirely recovered in each cycle on HZSM-5 at 623 K (Figure 5c), consistent with previous results. S4,55 At each shortest contact time of 2.3 min, methanol conversion repeatedly returned to nearly zero, meaning fewer hydrocarbons retained inside the zeolite channel. Hence, these organic hydrocarbon pool molecules are virtually spatially delocalized and can "randomly walk" across the channels of the zeolite host, behaving as the "fluid hydrocarbon pool" (Figure 5d). Such "walk-in-channel" behavior of bulky hydrocarbons cannot appear on cavity-structured zeolites and zeotypes such as SAPO-34, wherein bulky hydrocarbons are "imprisoned" in the cages due to the constrained diffusion.

A Hypercycle. The full-spectrum molecular routes of methanol conversion are an ensemble of chain reactions

comprising a cascade of catalytic and autocatalytic events, leading collectively to a large interlinked reaction network (Figure 6). In general, this network goes through three stages: initiating (to build incipient autocatalyst), sustaining (operating by a hypercyclic subnetwork), and decaying (autocatalysis extinction).

The initiating stage arguably originates from nucleophilic substitution reaction, with DME as a more plausible nucleophile to attack the SMS, constructing the initial C–C containing species. Despite substantive evidence gathered, this is by no means conclusive (or exclusive), as other conceivable initial C–C building routes 41,45,49,56–60 may also exist and operate. The generated incipient olefins (i.e., initial autocatalysts) trigger the autocatalytic reaction via an olefins-based cycle.

To disentangle the hidden autocatalytic patterns, we now reinterpret MTH chemistry with the aid of a classic, sophisticated autocatalysis concept. For the olefins-based cycle, one olefin molecule (associated with its microenvironments) catalyzes the formation of two olefins in one catalytic loop; this process is typically called "selfish" autocatalysis. While for the MCP- and aromatics-based cycles, MCP (or aromatic species) catalyze the formation of not only themselves but also olefins; in turn, the formed olefin feeds the re-formation of MCP (or aromatics) to close an additional catalytic loop (Figure 6). Such a mutual catalysis process is referred to as cross-catalysis, with MCP (or aromatics) and olefins forming the cross-catalytic pair, running concurrently with, and being as competent as, olefins-based "selfish"

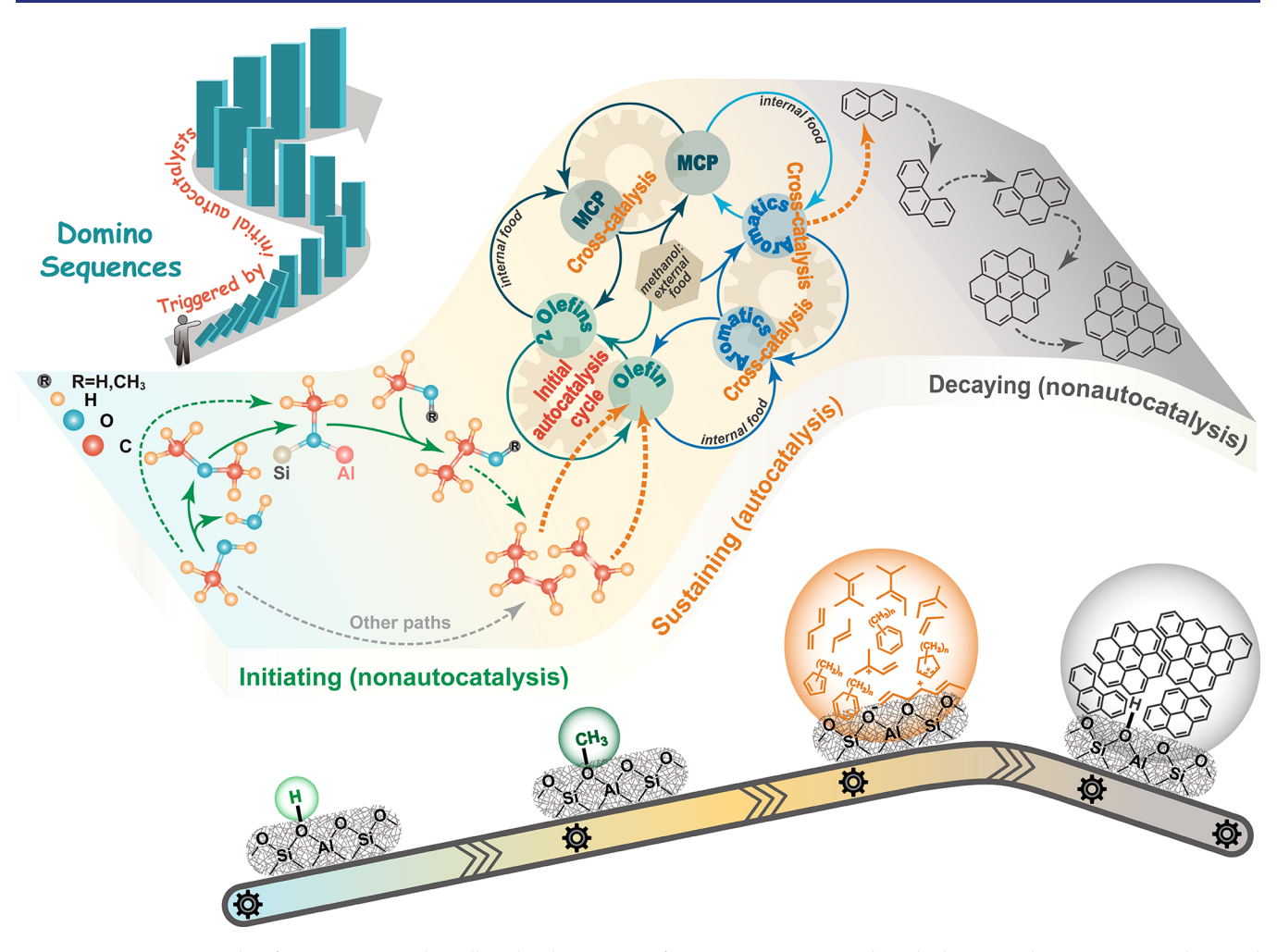


Figure 6. Domino cascade of reaction network. Full molecular picture of MTH reaction network with diverse and cooperative catalytic and autocatalytic events associated with the dynamic restructuring of active sites along the evolutionary trajectory. The autocatalytic sets, operating by a hypercyclic network embedded in the large interlinked network, interlinked by three autocatalytic entities (olefin, MCP, and aromatic species), driving the autocatalytic turnover. The actual mechanistic details of the reaction network may be more complex than the catalytic loops illustrated here.

autocatalysis. Likewise, another cross-catalysis is built between MCP and aromatics. Together, one olefins-based "selfish" autocatalytic cycle is coupled with other three cross-catalysis cycles (with olefinic, MCP, and aromatic species as autocatalytic entities) to forge a hypercycle, operating in concert to drive the autocatalytic turnover. The detailed molecular routes of this internally cycled hypercyclic network are depicted in Figure S20.

Concurrent with the dynamic development of the reaction network is the relay control of the active sites, which evolve from acidic protons to the SMS and then to organic—inorganic hybrid, microenvironment-involved supramolecular active centers. Eventually, those active aromatic species in the hypercycle gradually decay and age into on-surface or inpore inactive polycyclic aromatic hydrocarbons, terminating autocatalysis. The reaction sequence runs from the initiation to decay like dominoes. Incipient olefins-initiated domino sequences integrate multiple parallel and/or interactive elementary events, so the methanol conversion presents dynamically evolving molecular routes and a multistep reaction network.

Zeolite confined space imposes conspicuous effects on the initiating, sustaining, and decaying of autocatalytic cycles.

Zeolite pore space serves as the primary tool to modulate the formation and reactivity of effective autocatalysts (lighter olefins and cyclic species). Small pore sizes, e.g., of 8MR channeled zeolites, are unable to generate autocatalysts to ignite autocatalytic reactions. 63 The pores or intersections of 1D and 2D 10MR zeolites are able to initiate autocatalytic reactions. However, the pore or intersection sizes are not large enough to readily form cyclic autocatalysts, and the cracking of C₅⁺ aliphatic hydrocarbons to lighter olefin autocatalysts needs to overcome the higher energy barriers, resulting in the slow induction of autocatalytic reactivity.^{64,65} The intersections of 3D 10MR zeolites (such as HZSM-5)^{26,66-68} and 12 MR zeolites^{25,69,70} and cavities of cavity-structured zeolites^{71–74} are large enough to parallelly operate olefins-based and cyclicspecies-based autocatalytic cycles, with the chemical identity of cyclic autocatalysts varying with intersection/cavity sizes. However, the larger intersection ¹⁴ and cavity ⁷¹ facilitate the secondary catalytic reactions, leading to the formation of inactive polyaromatics and the rapid decaying of autocatalytic cycles. Moreover, more open space such as the half-supercage (surface pocket) of HMCM-22 zeolite and the external surface of common zeolites disfavors the aromatic dealkylation reactions,⁷⁵ thus being a disadvantage for the cyclic-speciesbased cycles but being an advantage for coking. Therefore, suitable pore space is the primary (or imperative) factor for initiating and efficiently sustaining the autocatalytic cycles (Figure S21a). Furthermore, the autocatalytic cycles dynamically evolve as reaction proceeds. Generally, the olefins-based cycle prevails over the induction and deactivation stages and the cyclic-species-based cycles dominate in the highly efficient reaction stage $^{76-78}$ (Figure S21b).

The diversity of zeolite pore space provides diverse autocatalytic routes. For each zeolite, the microenvironments (constituted of acidity and its surrounding confined space) customize the unique autocatalytic routes, but the reaction conditions, especially reaction temperature, can impose significant effects on the mechanistic orientation. Generally, methanol conversion over zeolite with lower acidity density at higher temperature favors the olefins-based autocatalytic cvcle; 54,79 however, methanol conversion over zeolite with higher acidity density at lower temperature favors the cyclicspecies-based cycles 76 (Figure S21c). Besides, the deactivating species at lower temperature may act as the active species at higher temperature. So,81 Thus, the zeolite confined space, acidity, and reaction conditions work together-in a cooperative manner—to dynamically modulate the operation of different autocatalytic and catalytic cycles. The multifactordetermined autocatalytic mechanism routes complicate the cycle/network regulation, but they provide more space or possibilities for catalyst design and product selectivity control.

CONCLUSION

By a multitechnique approach and multiscale analysis, this work addresses the long-standing search for a complete mechanistic framework of autocatalysis in a zeolite confined space, taking the MTH reaction as a prototype. First, DME (relative to methanol) is verified as the more active C1 species for building the initial C-C bond by multicharacterizations and calculations. Then, the reaction of DME with the SMS is experimentally and theoretically validated as the more plausible mechanistic pathway to generate the initial olefins. The formed initial olefins function as the "switch" to trigger the autocatalysis and drive the efficient conversion of methanol by gradually forming MCP and aromatic cyclic species. The progressive buildup/accumulation of highly operative autocatalysts explains the induction of autocatalysis. These in-built olefins and cyclic organic species are in synergy with inorganic zeolite microenvironments, acting as the true active centers. Those supramolecular active centers are dynamic and fluid, as the organic hydrocarbon pool molecules are validated to "randomly walk" across the channels of the zeolite host, behaving as the "fluid hydrocarbon pool".

By virtue of the classic autocatalysis concept, we unravel the chemical nature of an autocatalytic reaction network: one "selfish" autocatalysis cycle (olefins-based cycle) interlinked with three cross-catalysis cycles (with olefin, MCP, and aromatic species as autocatalytic entities), cooperatively constituting a hypercycle that efficiently drives and sustains autocatalysis. Together, we uncover a domino cascade of the MTH reaction network that is continuously evolved along the reaction course with initiating (to build incipient autocatalysts), sustaining (operating by a hypercyclic subnetwork), and decaying (autocatalysis extinction).

The autocatalytic chemistry in the exemplified MTH reaction reflects a dynamic process of C-C assembly (from C1 species to multicarbon products) and rearrangement of the

covalent bond. These processes are chemically driven by the proton acid catalysis and autocatalysis mediated by the supramolecular active centers in the zeolite confined space. The dynamic autocatalytic cycles/network uncovered here enrich our knowledge of the autocatalytic mechanism and its dynamic properties, and they can also serve as the fundamental basis for realizing the ultimate goal of the delicate control of the reaction process.

METHODS

Catalyst and Characterizations. The commercial NaZSM-5 samples were provided by the Catalyst Plant of Nankai University. HZSM-5 samples with Si/Al ratios of 15 and 90 were obtained through the following procedures: ion exchange was carried out in 1.0 mol $\rm L^{-1}$ NH $_4$ NO $_3$ aqueous solution at 353 K for 2 h for three times, followed by filtration, washing, and drying, and finally calcination at 823 K for 4 h. The catalyst characterizations, including powder X-ray diffraction (XRD), scanning electron microscopy (SEM), N $_2$ adsorption, and NH $_3$ temperature-programmed desorption (NH $_3$ -TPD), are shown in Figures S1–S3 and Table S1.

Catalytic Testing. All MTH and DTH reactions were carried out under atmospheric pressure by using a fixed-bed quartz tube reactor with an inner diameter of 4 mm. The HZSM-5 catalyst powder was extruded and sieved into 40–60 mesh. Prior to reaction, the catalyst was activated under He flow at 723 K for 40 min, and then the temperature was decreased to the reaction temperature. For every group of comparative experiments between MTH and DTH reactions, equimolar carbon amounts of methanol and DME were fed.

Activity test and cofeeding experiments were conducted at varied contact times. Typically, 5–100 mg of HZSM-5-90 catalysts was diluted with 238–0 mg of quartz sand (40–60 mesh) to keep the same bed volume. Gaseous DME (9 mol % dilution with helium) was directly fed at atmospheric pressure. CH₃OH (>99.8%) and H₂O (ultrapure grade) were fed by passing nitrogen through a saturation evaporator kept at 300 K for CH₃OH and 273–317 K for H₂O. The contact time range in activity test was 0.019–1.88 g_{cat.} h mol⁻¹. In cofeeding experiments, the partial pressure ratio of DME/H₂O was about 15:1–1:1 and the contact time was about 0.017–1.41 g_{cat.} h mol⁻¹.

Gaseous reaction products were kept at 473 K to avoid condensation and analyzed via an online gas chromatograph—mass spectrometer (GC–MS, Agilent 7890B/5977A) with a PoraPLOT Q capillary column and a flame ionization detector. The conversion and selectivity of the MTH and DTH reactions were calculated on a $\rm CH_2$ basis.

DRIFT Measurements. DRIFT spectra were obtained on a Bruker Tensor 27 instrument with a diffuse reflectance infrared cell with a ZnSe window and a liquid nitrogen cooled Hg–Cd–Te detector. The absorbance spectra were obtained by averaging 16 scans collected at 4 cm⁻¹ resolution. Gaseous reaction products were detected by online mass spectrometry. Prior to the measurements, 15 mg of catalyst powder was loaded into the cell, pre-treated under a He flow at 773 K for 60 min and, subsequently, decreased to reaction temperature. CH₃OH was fed by passing 4.4 mL/min nitrogen through a saturator evaporator kept at 275.4 K. DME (2.2 mol % dilution with helium) at 5 mL/min was fed at atmospheric pressure to give the same CH₂-based WHSV as CH₃OH.

For *in situ* TPD-DRIFT experiments, the activated catalyst was exposed to reactants at 393 K for 15 min to achieve adsorption saturation, followed by sweeping nitrogen (60 mL/min) for 30 min to remove the weakly adsorbed reactants. Then the cell was heated to 623 K with a heating rate of 3 K/min under 30 mL/min nitrogen sweeping.

For operando DRIFT experiments, the evolution of catalyst surface species as well as the gaseous products were simultaneously monitored by using an operando approach combining IR spectroscopy with online MS (Pfeiffer Omnistar GSD 301 T3). IR spectra and MS signal were simultaneously collected at 623 K as the reaction proceeded. According to the database of the National Institute of

Standards and Technology (NIST), the m/z values of the corresponding substances were as follows: methanol, 31 (after subtracting the fragment ion signal of m/z 31 from DME); DME, 45; ethylene, 26 (after subtracting the fragment ion signal of m/z 26 from propene); propene, 41 (after subtracting the fragment ion signal of m/z 41 from DME).

Solid-State NMR Experiments. Solid-state NMR (ssNMR) measurements were performed at 14.1 T on a Bruker 600 MHz widebore magnet with an AVANCE-III console, equipped with a 4 mm WVT magic angle spinning (MAS) probe or a 7 mm high temperature MAS-CAT probe, with resonance frequencies of 150.9 and 600.13 MHz for ¹³C and ¹H nuclei, respectively. Referencing chemical shifts were to adamantane with the upfield methine peak at 29.5 ppm.

For in situ ssNMR experiments, 82 about 200 mg of HZSM-5-90 sample was pre-dehydrated at 673 K for 20 h under vacuum (<10⁻³ Pa) and loaded into a 7 mm MAS NMR rotor reactor by pressing into a hollow cylinder using a specially constructed tool in a glovebox filled with dry nitrogen. After the rotor reactor was transferred to the 7 mm MAS-CAT probe (high temperature MAS NMR probe), the catalyst was activated at 573 K for 1 h under 40 mL/min helium flow and then introduced into the spinning MAS rotor via the injection tube. Subsequently, ¹³C-CH₃OH or ¹³C-DME was continuously fed into the MAS NMR rotor and in situ solid-state ¹³C MAS NMR spectra were recorded using one pulse sequence with a spinning rate of 3 kHz. ¹³C-CH₃OH was fed by passing helium through a saturator evaporator kept at 287 K with a CH₂-based WHSV of 4.8×10^{-2} mol_{CH}, h⁻¹ g_{cat.}⁻¹. ¹³C-DME (4.44 mol % dilution with helium) was fed with the same CH2-based WHSV and total flow rate as CH2OH. After in situ ssNMR experiments, the catalysts were transferred into a 4 mm WVT MAS probe, and 1D ¹H-¹³C cross-polarization (CP) spectra were recorded with a MAS frequency of 12 kHz and an accumulation of 1000 scans.

 $2D^{13}C-^{13}C$ CORD (combined $R2_{\nu}^{n}$ -driven) spin diffusion MAS NMR spectra were recorded at a spinning rate of 12 kHz with a 1 s recycle delay, 200 ms for the spin diffusion mixing time, and 576 and 168 scans for direct and indirect ^{13}C dimensions, respectively, and the typical 90° pulse lengths were 4.1 μs for ^{1}H and 3.6 μs for ^{13}C , respectively. The $^{1}H \rightarrow ^{13}C$ cross-polarization was performed by a linear amplitude ramp (50–100%) on ^{13}C with a 1 ms CP contact time. The general pulse sequence for 2D $^{13}C-^{13}C$ CORD homonuclear correlation experiments is shown in ref 83.

Theoretical Calculations. For all theoretical calculations, the HZSM-5 zeolite model is constructed by substituting an Al atom for a Si atom at the T12 site of the MFI structure.

Density functional theory (DFT) calculations performed with the Gaussian 09 software package were applied to calculate the adsorption energies of methanol, DME, and water, and a 72 T atom cluster model of HZSM-5 was used. The geometries of various adsorption structures were predicted by the combined theoretical method, i.e., ONIOM (ω B97XD/6-31G(d,p):AM1). The ω B97XD method developed by Chai and Head-Gordon covers empirical dispersion and can describe long-range dispersion interactions. In the ONIOM simulations, in the high-level layer, the adsorbed molecules and the atoms of the zeolite framework (24 T of HZSM-5) surrounding the adsorbate were relaxed. The atoms in the low-level layer were fixed at their crystallographic locations. Frequency calculations are performed by using the ONIOM (ω B97XD/6-31G(d,p):AM1) method. Then, the single-point energies were obtained at the level of ω B97XD/6-31G(d,p).

PDOS and the energies of HESBF for reactants were calculated by a 62 T atom cluster model using the Vienna Ab initio Simulation Package (VASP). The generalized gradient approximation (GGA) in the form of the revised Perdew–Burke–Ernzerhof (revPBE) functional was adopted for the exchange–correlation interactions. B8,89 During structural optimization, the convergence criterion for the residual force on each atom was set to 0.05 eV/Å and the cutoff energy for the plane wave was set to 400 eV. A gamma-centered k-point sampling $1 \times 1 \times 1$ was used for the Brillouin zone integration. Grimme's dispersion corrections (DFT-D3) 90 were used to consider

the dispersion interaction, and a Gaussian smearing with a width of 0.2 eV was used. On the basis of the optimized configurations, the PDOS and the energies of HESBF for the reactants were further calculated with the gamma-centered k-point $3 \times 3 \times 3$.

For the theoretical calculation of the initial C-C bond formation, the unit cell of HZSM-5 (96 T atoms) was used. In this part, all geometrical optimizations by DFT calculations and AIMD simulations were performed with the CP2K simulation software package. The PBE functional⁸⁸ was used with the DZVP-GTH basis set⁹² and with the dispersion correction to energy and forces due to the DFT-D3⁹⁰ method. The time step of integration was set as 0.5 fs. Periodic DFT was selected to optimize the geometrical structures and cell parameters. After insertion of the guest molecules inside the zeolite channels, the system was further optimized as the initial state of reactants, and subsequently, 5 ps molecular dynamics simulation in the isothermal-isobaric ensemble (NPT) was applied to relax the structure and cell at 673 K and 1 bar. The activation of methanol and DME by the SMS as well as the formation of the initial C-C bond, which is a rare event, was investigated by using metadynamics (MTD) simulations at 673 K in the canonical ensemble (NVT), using the relaxed cell parameters from the previous NPT simulation. The MTD method was developed by Laio and Parrinello and is an advanced sampling technique used to enhance the probability of sampling chemical reactions or rare events. 93–95 During the MTD simulation, Gaussian hills were regularly spawned along the chosen collective variable(s), which were defined by coordination numbers (CNs):

$$CN = \sum_{ij} \frac{1 - \left(\frac{r_{ij} - d_0}{r_0}\right)^m}{1 - \left(\frac{r_{ij} - d_0}{r_0}\right)^m}$$
(4)

The sum in eq 4 runs over two sets of atoms, i and j; r_{ii} is the interatomic distance between atoms i and j; r_0 is a reference distance. In this study, the parameters d_0 , n, and m were set to 0, 6, and 12, respectively. The construction of the initial C-C bond from direct coupling of the SMS with methanol/DME relates to the formation and rupture of multiple bonds between C, H, and O, and the best collective variables (CVs) with numerous attempts to drive the reaction pathways are depicted in Scheme S1. The first collective variable (CV1) is defined by the CN between the surface methoxy's carbon (Cs) and the four zeolite oxygen atoms (Oz) bonded to the Al atom, i.e., CV1 = CN(Cs-Oz). A reference distance r_0 of 2.1 Å was chosen for CN(Cs-Oz). The second collective variable (CV2) is defined by the CN between Cs and the reactant carbon atoms (Cr), i.e., CV2 = CN(Cs-Cr). A reference distance of CN(Cs-Cr) was 1.5 Å. Hills with widths of 0.035 and 0.045 for CV1 and CV2 were spawned every 100 time steps, and the height of the Gaussian hills was set to 3 kJ/mol. The simulations proceeded until the height of the additional hills no longer influenced the resulting free energy profile. Based on the sum of the spawned Gaussian hills, the 2D free energy profile of the reaction was reconstructed, and the lowest free energy path was calculated by MEPSA software.9

ASSOCIATED CONTENT

Supporting Information

The Supporting Information is available free of charge at https://pubs.acs.org/doi/10.1021/jacs.1c03475.

Characterization results (XRD, SEM, NH₃-TPD), detailed derivation and hypothesis of the autocatalytic kinetic model, other supplementary results and discussions of reaction and spectroscopy (PDF)

AUTHOR INFORMATION

Corresponding Authors

Zhongmin Liu – National Engineering Laboratory for Methanol to Olefins, Dalian National Laboratory for Clean Energy, iChEM (Collaborative Innovation Center of Chemistry for Energy Materials) and State Key Laboratory of Catalysis, Dalian Institute of Chemical Physics, Chinese Academy of Sciences, Dalian 116023, People's Republic of China; University of Chinese Academy of Sciences, Beijing 100049, People's Republic of China; orcid.org/0000-0002-7999-2940; Email: liuzm@dicp.ac.cn

Yingxu Wei — National Engineering Laboratory for Methanol to Olefins, Dalian National Laboratory for Clean Energy, iChEM (Collaborative Innovation Center of Chemistry for Energy Materials), Dalian Institute of Chemical Physics, Chinese Academy of Sciences, Dalian 116023, People's Republic of China; Email: weiyx@dicp.ac.cn

Anmin Zheng — National Center for Magnetic Resonance in Wuhan, State Key Laboratory of Magnetic Resonance and Atomic and Molecular Physics, Key Laboratory of Magnetic Resonance in Biological Systems, Wuhan Institute of Physics and Mathematics, Innovation Academy for Precision Measurement Science and Technology, Chinese Academy of Sciences, Wuhan 430071, People's Republic of China; orcid.org/0000-0001-7115-6510; Email: zhenganm@wipm.ac.cn

Jianping Xiao — University of Chinese Academy of Sciences, Beijing 100049, People's Republic of China; State Key Laboratory of Catalysis, Dalian Institute of Chemical Physics, Chinese Academy of Sciences, Dalian 116023, People's Republic of China; Orcid.org/0000-0003-1779-6140; Email: xiao@dicp.ac.cn

Authors

Shanfan Lin — National Engineering Laboratory for Methanol to Olefins, Dalian National Laboratory for Clean Energy, iChEM (Collaborative Innovation Center of Chemistry for Energy Materials), Dalian Institute of Chemical Physics, Chinese Academy of Sciences, Dalian 116023, People's Republic of China; University of Chinese Academy of Sciences, Beijing 100049, People's Republic of China

Yuchun Zhi — National Engineering Laboratory for Methanol to Olefins, Dalian National Laboratory for Clean Energy, iChEM (Collaborative Innovation Center of Chemistry for Energy Materials), Dalian Institute of Chemical Physics, Chinese Academy of Sciences, Dalian 116023, People's Republic of China

Wei Chen — National Center for Magnetic Resonance in Wuhan, State Key Laboratory of Magnetic Resonance and Atomic and Molecular Physics, Key Laboratory of Magnetic Resonance in Biological Systems, Wuhan Institute of Physics and Mathematics, Innovation Academy for Precision Measurement Science and Technology, Chinese Academy of Sciences, Wuhan 430071, People's Republic of China; orcid.org/0000-0002-8955-9497

Huan Li – University of Chinese Academy of Sciences, Beijing 100049, People's Republic of China; State Key Laboratory of Catalysis, Dalian Institute of Chemical Physics, Chinese Academy of Sciences, Dalian 116023, People's Republic of China

Wenna Zhang — National Engineering Laboratory for Methanol to Olefins, Dalian National Laboratory for Clean Energy, iChEM (Collaborative Innovation Center of Chemistry for Energy Materials), Dalian Institute of Chemical Physics, Chinese Academy of Sciences, Dalian 116023, People's Republic of China

Caiyi Lou – National Engineering Laboratory for Methanol to Olefins, Dalian National Laboratory for Clean Energy, iChEM (Collaborative Innovation Center of Chemistry for Energy Materials), Dalian Institute of Chemical Physics, Chinese Academy of Sciences, Dalian 116023, People's Republic of China; University of Chinese Academy of Sciences, Beijing 100049, People's Republic of China

Xinqiang Wu — National Engineering Laboratory for Methanol to Olefins, Dalian National Laboratory for Clean Energy, iChEM (Collaborative Innovation Center of Chemistry for Energy Materials), Dalian Institute of Chemical Physics, Chinese Academy of Sciences, Dalian 116023, People's Republic of China

Shu Zeng — National Engineering Laboratory for Methanol to Olefins, Dalian National Laboratory for Clean Energy, iChEM (Collaborative Innovation Center of Chemistry for Energy Materials), Dalian Institute of Chemical Physics, Chinese Academy of Sciences, Dalian 116023, People's Republic of China; University of Chinese Academy of Sciences, Beijing 100049, People's Republic of China

Shutao Xu — National Engineering Laboratory for Methanol to Olefins, Dalian National Laboratory for Clean Energy, iChEM (Collaborative Innovation Center of Chemistry for Energy Materials), Dalian Institute of Chemical Physics, Chinese Academy of Sciences, Dalian 116023, People's Republic of China; orcid.org/0000-0003-4722-8371

Complete contact information is available at: https://pubs.acs.org/10.1021/jacs.1c03475

Author Contributions

[⊥]S. Lin and Y. Zhi contributed equally.

Notes

The authors declare no competing financial interest.

ACKNOWLEDGMENTS

We thank the National Natural Science Foundation of China (Grant Nos. 22072148, 21703239, 21991092, and 22032005), DICP I202121, the High Level Talents Innovative Support Plan of Dalian (2019RQ031), the Key Research Program of Frontier Sciences, Chinese Academy of Sciences (QYZDY-SSW-SC024), and the International Partnership Program of Chinese Academy of Sciences (121421KYSB20180007) for financial support.

■ REFERENCES

- (1) Bissette, A. J.; Fletcher, S. P. Mechanisms of Autocatalysis. *Angew. Chem., Int. Ed.* **2013**, 52 (49), 12800–12826.
- (2) Gadgil, C. J.; Kulkarni, B. D. Autocatalysis in biological systems. *AIChE J.* **2009**, *SS* (3), *SS6*–*S62*.
- (3) Miras, H. N.; Mathis, C.; Xuan, W.; Long, D.-L.; Pow, R.; Cronin, L. Spontaneous formation of autocatalytic sets with self-replicating inorganic metal oxide clusters. *Proc. Natl. Acad. Sci. U. S. A.* **2020**, *117* (20), 10699–10705.
- (4) Ottelé, J.; Hussain, A. S.; Mayer, C.; Otto, S. Chance emergence of catalytic activity and promiscuity in a self-replicator. *Nat. Catal.* **2020**, *3* (7), 547–553.
- (5) Jogunola, O.; Salmi, T.; Eränen, K.; Wärnå, J.; Mikkola, J. P. Rates and equilibria of ester hydrolysis: Combination of slow and rapid reactions. *Chem. Eng. Process.* **2011**, *50* (7), *665–674*.
- (6) Luisi, P. L. The Emergence of Life: From Chemical Origins to Synthetic Biology; Cambridge University Press: 2006.
- (7) Küchler, A.; Yoshimoto, M.; Luginbühl, S.; Mavelli, F.; Walde, P. Enzymatic reactions in confined environments. *Nat. Nanotechnol.* **2016**, *11* (5), 409–420.

- (8) Gounder, R.; Iglesia, E. The catalytic diversity of zeolites: confinement and solvation effects within voids of molecular dimensions. *Chem. Commun.* **2013**, *49* (34), 3491–3509.
- (9) Fu, Q.; Bao, X. Confined microenvironment for catalysis control. *Nat. Catal.* **2019**, 2 (10), 834–836.
- (10) Chang, C. D.; Silvestri, A. J. The conversion of methanol and other O-compounds to hydrocarbons over zeolite catalysts. *J. Catal.* **1977**, 47 (2), 249–259.
- (11) Chen, N. Y.; Reagan, W. J. Evidence of autocatalysis in methanol to hydrocarbon reactions over zeolite catalysts. *J. Catal.* **1979**, *59* (1), 123–129.
- (12) Dessau, R. M.; LaPierre, R. B. On the mechanism of methanol conversion to hydrocarbons over HZSM-5. *J. Catal.* **1982**, 78 (1), 136–141.
- (13) Dessau, R. M. On the H-ZSM-5 catalyzed formation of ethylene from methanol or higher olefins. *J. Catal.* **1986**, 99 (1), 111–116
- (14) Bleken, F.; Skistad, W.; Barbera, K.; Kustova, M.; Bordiga, S.; Beato, P.; Lillerud, K. P.; Svelle, S.; Olsbye, U. Conversion of methanol over 10-ring zeolites with differing volumes at channel intersections: comparison of TNU-9, IM-5, ZSM-11 and ZSM-5. *Phys. Chem. Chem. Phys.* **2011**, *13* (7), 2539–2549.
- (15) Mole, T.; Whiteside, J. A.; Seddon, D. Aromatic co-catalysis of methanol conversion over zeolite catalysts. *J. Catal.* **1983**, 82 (2), 261–266.
- (16) Mole, T.; Bett, G.; Seddon, D. Conversion of methanol to hydrocarbons over ZSM-5 zeolite: An examination of the role of aromatic hydrocarbons using ¹³carbon- and deuterium-labeled feeds. *J. Catal.* **1983**, *84* (2), 435–445.
- (17) Dahl, I. M.; Kolboe, S. On the reaction mechanism for propene formation in the MTO reaction over SAPO-34. *Catal. Lett.* **1993**, 20 (3), 329–336.
- (18) Dahl, I. M.; Kolboe, S. On the Reaction Mechanism for Hydrocarbon Formation from Methanol over SAPO-34: I. Isotopic Labeling Studies of the Co-Reaction of Ethene and Methanol. *J. Catal.* **1994**, 149 (2), 458–464.
- (19) Dahl, I. M.; Kolboe, S. On the Reaction Mechanism for Hydrocarbon Formation from Methanol over SAPO-34:2. Isotopic Labeling Studies of the Co-reaction of Propene and Methanol. *J. Catal.* **1996**, *161* (1), 304–309.
- (20) Arstad, B.; Kolboe, S. The Reactivity of Molecules Trapped within the SAPO-34 Cavities in the Methanol-to-Hydrocarbons Reaction. *J. Am. Chem. Soc.* **2001**, *123* (33), 8137–8138.
- (21) Song, W.; Haw, J. F.; Nicholas, J. B.; Heneghan, C. S. Methylbenzenes Are the Organic Reaction Centers for Methanol-to-Olefin Catalysis on HSAPO-34. *J. Am. Chem. Soc.* **2000**, *122* (43), 10726–10727.
- (22) Haw, J. F.; Marcus, D. M. Well-defined (supra)molecular structures in zeolite methanol-to-olefin catalysis. *Top. Catal.* **2005**, *34* (1), 41–48.
- (23) Sassi, A.; Wildman, M. A.; Ahn, H. J.; Prasad, P.; Nicholas, J. B.; Haw, J. F. Methylbenzene Chemistry on Zeolite HBeta: Multiple Insights into Methanol-to-Olefin Catalysis. *J. Phys. Chem. B* **2002**, *106* (9), 2294–2303.
- (24) Sassi, A.; Wildman, M. A.; Haw, J. F. Reactions of Butylbenzene Isomers on Zeolite HBeta: Methanol-to-Olefins Hydrocarbon Pool Chemistry and Secondary Reactions of Olefins. *J. Phys. Chem. B* **2002**, 106 (34), 8768–8773.
- (25) Bjørgen, M.; Akyalcin, S.; Olsbye, U.; Benard, S.; Kolboe, S.; Svelle, S. Methanol to hydrocarbons over large cavity zeolites: Toward a unified description of catalyst deactivation and the reaction mechanism. *J. Catal.* **2010**, 275 (1), 170–180.
- (26) Svelle, S.; Joensen, F.; Nerlov, J.; Olsbye, U.; Lillerud, K.-P.; Kolboe, S.; Bjørgen, M. Conversion of Methanol into Hydrocarbons over Zeolite H-ZSM-5: Ethene Formation Is Mechanistically Separated from the Formation of Higher Alkenes. *J. Am. Chem. Soc.* **2006**, *128* (46), 14770–14771.
- (27) Bjørgen, M.; Svelle, S.; Joensen, F.; Nerlov, J.; Kolboe, S.; Bonino, F.; Palumbo, L.; Bordiga, S.; Olsbye, U. Conversion of

- methanol to hydrocarbons over zeolite H-ZSM-5: On the origin of the olefinic species. *J. Catal.* **2007**, 249 (2), 195–207.
- (28) Bjørgen, M.; Lillerud, K.-P.; Olsbye, U.; Svelle, S. Conversion of methanol to hydrocarbons: Hints to rational catalyst design from fundamental mechanistic studies on H-ZSM-5. *Stud. Surf. Sci. Catal.* **2007**, *167*, 463–468.
- (29) Bjørgen, M.; Joensen, F.; Lillerud, K.-P.; Olsbye, U.; Svelle, S. The mechanisms of ethene and propene formation from methanol over high silica H-ZSM-5 and H-beta. *Catal. Today* **2009**, *142* (1), 90–97.
- (30) Zhang, W.; Zhi, Y.; Huang, J.; Wu, X.; Zeng, S.; Xu, S.; Zheng, A.; Wei, Y.; Liu, Z. Methanol to Olefins Reaction Route Based on Methylcyclopentadienes as Critical Intermediates. *ACS Catal.* **2019**, *9* (8), 7373–7379.
- (31) Yarulina, I.; Chowdhury, A. D.; Meirer, F.; Weckhuysen, B. M.; Gascon, J. Recent trends and fundamental insights in the methanol-to-hydrocarbons process. *Nat. Catal.* **2018**, *1* (6), 398–411.
- (32) Xu, S.; Zhi, Y.; Han, J.; Zhang, W.; Wu, X.; Sun, T.; Wei, Y.; Liu, Z. Advances in Catalysis for Methanol-to-Olefins Conversion. *Adv. Catal.* **2017**, *61*, 37–122.
- (33) Blackmond, D. G. Autocatalytic Models for the Origin of Biological Homochirality. *Chem. Rev.* **2020**, *120* (11), 4831–4847.
- (34) Martinez-Espin, J. S.; Mortén, M.; Janssens, T. V. W.; Svelle, S.; Beato, P.; Olsbye, U. New insights into catalyst deactivation and product distribution of zeolites in the methanol-to-hydrocarbons (MTH) reaction with methanol and dimethyl ether feeds. *Catal. Sci. Technol.* **2017**, *7* (13), 2700–2716.
- (35) Chang, C. D. A kinetic model for methanol conversion to hydrocarbons. *Chem. Eng. Sci.* **1980**, 35 (3), 619–622.
- (36) Ono, Y.; Mori, T. Mechanism of methanol conversion into hydrocarbons over ZSM-5 zeolite. *J. Chem. Soc., Faraday Trans.* 1 1981, 77 (9), 2209–2221.
- (37) Márquez, F.; García, H.; Palomares, E.; Fernández, L.; Corma, A. Spectroscopic Evidence in Support of the Molecular Orbital Confinement Concept: Case of Anthracene Incorporated in Zeolites. *J. Am. Chem. Soc.* **2000**, 122 (27), 6520–6521.
- (38) Sastre, G.; Viruela, P. M.; Corma, A. Quantum chemistry calculations on the effect of electron confinement upon the frontier molecular orbitals of ethylene and benzene in sodalite. Implications on reactivity. *Chem. Phys. Lett.* **1997**, 264 (6), 565–572.
- (39) Ivanova, I. I.; Corma, A. Surface Species Formed and Their Reactivity during the Alkylation of Toluene by Methanol and Dimethyl Ether on Zeolites As Determined by in Situ ¹³C MAS NMR. *J. Phys. Chem. B* **1997**, *101* (4), 547–551.
- (40) Wang, W.; Seiler, M.; Hunger, M. Role of Surface Methoxy Species in the Conversion of Methanol to Dimethyl Ether on Acidic Zeolites Investigated by in Situ Stopped-Flow MAS NMR Spectroscopy. *J. Phys. Chem. B* **2001**, *105* (50), 12553–12558.
- (41) Wu, X.; Xu, S.; Zhang, W.; Huang, J.; Li, J.; Yu, B.; Wei, Y.; Liu, Z. Direct Mechanism of the First Carbon-Carbon Bond Formation in the Methanol-to-Hydrocarbons Process. *Angew. Chem., Int. Ed.* **2017**, 56 (31), 9039–9043.
- (42) Campbell, S. M.; Jiang, X.-Z.; Howe, R. F. Methanol to hydrocarbons: spectroscopic studies and the significance of extra-framework aluminium. *Microporous Mesoporous Mater.* **1999**, 29 (1), 91–108.
- (43) Forester, T. R.; Howe, R. F. In situ FTIR studies of methanol and dimethyl ether in ZSM-5. *J. Am. Chem. Soc.* **1987**, *109* (17), 5076–5082.
- (44) Wu, X.; Xu, S.; Wei, Y.; Zhang, W.; Huang, J.; Xu, S.; He, Y.; Lin, S.; Sun, T.; Liu, Z. Evolution of C-C Bond Formation in the Methanol-to-Olefins Process: From Direct Coupling to Autocatalysis. *ACS Catal.* **2018**, *8* (8), 7356–7361.
- (45) Chu, Y.; Yi, X.; Li, C.; Sun, X.; Zheng, A. Brønsted/Lewis acid sites synergistically promote the initial C-C bond formation in the MTO reaction. *Chem. Sci.* **2018**, *9* (31), 6470–6479.
- (46) Zhi, Y.; Shi, H.; Mu, L.; Liu, Y.; Mei, D.; Camaioni, D. M.; Lercher, J. A. Dehydration Pathways of 1-Propanol on HZSM-5 in the

- Presence and Absence of Water. J. Am. Chem. Soc. 2015, 137 (50), 15781-15794.
- (47) Mirth, G.; Lercher, J. A.; Anderson, M. W.; Klinowski, J. Adsorption complexes of methanol on zeolite ZSM-5. *J. Chem. Soc., Faraday Trans.* **1990**, *86* (17), 3039–3044.
- (48) Wang, W.; Hunger, M. Reactivity of Surface Alkoxy Species on Acidic Zeolite Catalysts. *Acc. Chem. Res.* **2008**, *41* (8), 895–904.
- (49) Chowdhury, A. D.; Houben, K.; Whiting, G. T.; Mokhtar, M.; Asiri, A. M.; Al-Thabaiti, S. A.; Basahel, S. N.; Baldus, M.; Weckhuysen, B. M. Initial Carbon-Carbon Bond Formation during the Early Stages of the Methanol-to-Olefin Process Proven by Zeolite-Trapped Acetate and Methyl Acetate. *Angew. Chem., Int. Ed.* **2016**, *55* (51), 15840–15845.
- (50) Minova, I. B.; Matam, S. K.; Greenaway, A.; Catlow, C. R. A.; Frogley, M. D.; Cinque, G.; Wright, P. A.; Howe, R. F. Elementary Steps in the Formation of Hydrocarbons from Surface Methoxy Groups in HZSM-5 Seen by Synchrotron Infrared Microspectroscopy. *ACS Catal.* **2019**, *9* (7), 6564–6570.
- (51) Mosley, J. D.; Young, J. W.; Agarwal, J.; Schaefer, H. F., III; Schleyer, P. v. R.; Duncan, M. A. Structural Isomerization of the Gas-Phase 2-Norbornyl Cation Revealed with Infrared Spectroscopy and Computational Chemistry. *Angew. Chem., Int. Ed.* **2014**, *53* (23), 5888–5891.
- (52) Shao, S.; Zhang, H.; Xiao, R.; Li, X.; Cai, Y. Catalytic conversion of biomass-derivates by in situ DRIFTS: Evolution of coke. *J. Anal. Appl. Pyrolysis* **2017**, *127*, 258–268.
- (53) Wang, C.; Wang, Q.; Xu, J.; Qi, G.; Gao, P.; Wang, W.; Zou, Y.; Feng, N.; Liu, X.; Deng, F. Direct Detection of Supramolecular Reaction Centers in the Methanol-to-Olefins Conversion over Zeolite H-ZSM-5 by ¹³C-²⁷Al Solid-State NMR Spectroscopy. *Angew. Chem., Int. Ed.* **2016**, *55* (7), 2507–2511.
- (54) Sun, X.; Mueller, S.; Liu, Y.; Shi, H.; Haller, G. L.; Sanchez-Sanchez, M.; van Veen, A. C.; Lercher, J. A. On reaction pathways in the conversion of methanol to hydrocarbons on HZSM-5. *J. Catal.* **2014**, *317*, 185–197.
- (55) Olsbye, U.; Svelle, S.; Bjørgen, M.; Beato, P.; Janssens, T. V. W.; Joensen, F.; Bordiga, S.; Lillerud, K. P. Conversion of Methanol to Hydrocarbons: How Zeolite Cavity and Pore Size Controls Product Selectivity. *Angew. Chem., Int. Ed.* **2012**, *51* (24), 5810–5831.
- (56) Li, J.; Wei, Z.; Chen, Y.; Jing, B.; He, Y.; Dong, M.; Jiao, H.; Li, X.; Qin, Z.; Wang, J.; Fan, W. A route to form initial hydrocarbon pool species in methanol conversion to olefins over zeolites. *J. Catal.* **2014**, 317, 277–283.
- (57) Comas-Vives, A.; Valla, M.; Copéret, C.; Sautet, P. Cooperativity between Al Sites Promotes Hydrogen Transfer and Carbon-Carbon Bond Formation upon Dimethyl Ether Activation on Alumina. ACS Cent. Sci. 2015, 1 (6), 313–319.
- (58) Liu, Y.; Müller, S.; Berger, D.; Jelic, J.; Reuter, K.; Tonigold, M.; Sanchez-Sanchez, M.; Lercher, J. A. Formation Mechanism of the First Carbon-Carbon Bond and the First Olefin in the Methanol Conversion into Hydrocarbons. *Angew. Chem., Int. Ed.* **2016**, *55* (19), 5723–5726.
- (59) Wang, C.; Chu, Y.; Xu, J.; Wang, Q.; Qi, G.; Gao, P.; Zhou, X.; Deng, F. Extra-Framework Aluminum-Assisted Initial C-C Bond Formation in Methanol-to-Olefins Conversion on Zeolite H-ZSM-5. *Angew. Chem., Int. Ed.* **2018**, *57* (32), 10197–10201.
- (60) Yang, L.; Yan, T.; Wang, C.; Dai, W.; Wu, G.; Hunger, M.; Fan, W.; Xie, Z.; Guan, N.; Li, L. Role of Acetaldehyde in the Roadmap from Initial Carbon-Carbon Bonds to Hydrocarbons during Methanol Conversion. *ACS Catal.* **2019**, *9* (7), 6491–6501.
- (61) Mores, D.; Stavitski, E.; Kox, M. H. F.; Kornatowski, J.; Olsbye, U.; Weckhuysen, B. M. Space- and Time-Resolved In-situ Spectroscopy on the Coke Formation in Molecular Sieves: Methanol-to-Olefin Conversion over H-ZSM-5 and H-SAPO-34. *Chem. Eur. J.* **2008**, *14* (36), 11320–11327.
- (62) Wang, N.; Zhi, Y.; Wei, Y.; Zhang, W.; Liu, Z.; Huang, J.; Sun, T.; Xu, S.; Lin, S.; He, Y.; Zheng, A.; Liu, Z. Molecular elucidating of an unusual growth mechanism for polycyclic aromatic hydrocarbons in confined space. *Nat. Commun.* **2020**, *11* (1), 1079.

- (63) Deimund, M. A.; Schmidt, J. E.; Davis, M. E. Effect of Pore and Cage Size on the Formation of Aromatic Intermediates During the Methanol-to-Olefins Reaction. *Top. Catal.* **2015**, *58* (7), 416–423.
- (64) Zhang, M.; Xu, S.; Wei, Y.; Li, J.; Chen, J.; Wang, J.; Zhang, W.; Gao, S.; Li, X.; Wang, C.; Liu, Z. Methanol conversion on ZSM-22, ZSM-35 and ZSM-5 zeolites: effects of 10-membered ring zeolite structures on methylcyclopentenyl cations and dual cycle mechanism. *RSC Adv.* **2016**, *6* (98), 95855–95864.
- (65) Teketel, S.; Skistad, W.; Benard, S.; Olsbye, U.; Lillerud, K. P.; Beato, P.; Svelle, S. Shape Selectivity in the Conversion of Methanol to Hydrocarbons: The Catalytic Performance of One-Dimensional 10-Ring Zeolites: ZSM-22, ZSM-23, ZSM-48, and EU-1. *ACS Catal.* **2012**, 2 (1), 26–37.
- (66) Svelle, S.; Olsbye, U.; Joensen, F.; Bjørgen, M. Conversion of Methanol to Alkenes over Medium- and Large-Pore Acidic Zeolites: Steric Manipulation of the Reaction Intermediates Governs the Ethene/Propene Product Selectivity. *J. Phys. Chem. C* **2007**, *111* (49), 17981–17984.
- (67) Wang, C.; Chu, Y.; Zheng, A.; Xu, J.; Wang, Q.; Gao, P.; Qi, G.; Gong, Y.; Deng, F. New Insight into the Hydrocarbon-Pool Chemistry of the Methanol-to-Olefins Conversion over Zeolite H-ZSM-5 from GC-MS, Solid-State NMR Spectroscopy, and DFT Calculations. *Chem. Eur. J.* 2014, 20 (39), 12432–12443.
- (68) Wang, C.; Yi, X.; Xu, J.; Qi, G.; Gao, P.; Wang, W.; Chu, Y.; Wang, Q.; Feng, N.; Liu, X.; Zheng, A.; Deng, F. Experimental Evidence on the Formation of Ethene through Carbocations in Methanol Conversion over H-ZSM-5 Zeolite. *Chem. Eur. J.* **2015**, 21 (34), 12061–12068.
- (69) Zhang, M.; Xu, S.; Li, J.; Wei, Y.; Gong, Y.; Chu, Y.; Zheng, A.; Wang, J.; Zhang, W.; Wu, X.; Deng, F.; Liu, Z. Methanol to hydrocarbons reaction over $H\beta$ zeolites studied by high resolution solid-state NMR spectroscopy: Carbenium ions formation and reaction mechanism. *J. Catal.* **2016**, 335, 47–57.
- (70) Teketel, S.; Olsbye, U.; Lillerud, K.-P.; Beato, P.; Svelle, S. Selectivity control through fundamental mechanistic insight in the conversion of methanol to hydrocarbons over zeolites. *Microporous Mesoporous Mater.* **2010**, *136* (1), 33–41.
- (71) Xu, S.; Zheng, A.; Wei, Y.; Chen, J.; Li, J.; Chu, Y.; Zhang, M.; Wang, Q.; Zhou, Y.; Wang, J.; Deng, F.; Liu, Z. Direct Observation of Cyclic Carbenium Ions and Their Role in the Catalytic Cycle of the Methanol-to-Olefin Reaction over Chabazite Zeolites. *Angew. Chem., Int. Ed.* **2013**, 52 (44), 11564–11568.
- (72) Li, J.; Wei, Y.; Chen, J.; Tian, P.; Su, X.; Xu, S.; Qi, Y.; Wang, Q.; Zhou, Y.; He, Y.; Liu, Z. Observation of Heptamethylbenzenium Cation over SAPO-Type Molecular Sieve DNL-6 under Real MTO Conversion Conditions. J. Am. Chem. Soc. 2012, 134 (2), 836–839.
- (73) Zhang, W.; Chen, J.; Xu, S.; Chu, Y.; Wei, Y.; Zhi, Y.; Huang, J.; Zheng, A.; Wu, X.; Meng, X.; Xiao, F.; Deng, F.; Liu, Z. Methanol to Olefins Reaction over Cavity-type Zeolite: Cavity Controls the Critical Intermediates and Product Selectivity. *ACS Catal.* **2018**, 8 (12), 10950–10963.
- (74) Zhou, J.; Zhi, Y.; Zhang, J.; Liu, Z.; Zhang, T.; He, Y.; Zheng, A.; Ye, M.; Wei, Y.; Liu, Z. Presituated "coke"-determined mechanistic route for ethene formation in the methanol-to-olefins process on SAPO-34 catalyst. *J. Catal.* **2019**, *377*, 153–162.
- (75) Khare, R.; Bhan, A. Mechanistic studies of methanol-to-hydrocarbons conversion on diffusion-free MFI samples. *J. Catal.* **2015**, 329, 218–228.
- (76) Hereijgers, B. P. C.; Bleken, F.; Nilsen, M. H.; Svelle, S.; Lillerud, K.-P.; Bjørgen, M.; Weckhuysen, B. M.; Olsbye, U. Product shape selectivity dominates the Methanol-to-Olefins (MTO) reaction over H-SAPO-34 catalysts. *J. Catal.* **2009**, 264 (1), 77–87.
- (77) Zhang, W.; Zhang, M.; Xu, S.; Gao, S.; Wei, Y.; Liu, Z. Methylcyclopentenyl Cations Linking Initial Stage and Highly Efficient Stage in Methanol-to-Hydrocarbon Process. *ACS Catal.* **2020**, *10* (8), 4510–4516.
- (78) Zhang, M.; Xu, S.; Wei, Y.; Li, J.; Wang, J.; Zhang, W.; Gao, S.; Liu, Z. Changing the balance of the MTO reaction dual-cycle

- mechanism: Reactions over ZSM-5 with varying contact times. *Chin. J. Catal.* **2016**, 37 (8), 1413–1422.
- (79) Yu, B.; Lou, C.; Zhang, W.; Xu, S.; Han, J.; Yu, Z.; Wei, Y.; Liu, Z. Insight into the Dual Cycle Mechanism of Methanol-to-Olefins Reaction over SAPO-34 Molecular Sieve by Isotopic Tracer Studies. *Chem. Res. Chin. Univ.* **2020**, *36* (6), 1203–1208.
- (80) Borodina, E.; Sharbini Harun Kamaluddin, H.; Meirer, F.; Mokhtar, M.; Asiri, A. M.; Al-Thabaiti, S. A.; Basahel, S. N.; Ruiz-Martinez, J.; Weckhuysen, B. M. Influence of the Reaction Temperature on the Nature of the Active and Deactivating Species During Methanol-to-Olefins Conversion over H-SAPO-34. ACS Catal. 2017, 7 (8), 5268–5281.
- (81) Goetze, J.; Meirer, F.; Yarulina, I.; Gascon, J.; Kapteijn, F.; Ruiz-Martínez, J.; Weckhuysen, B. M. Insights into the Activity and Deactivation of the Methanol-to-Olefins Process over Different Small-Pore Zeolites As Studied with Operando UV-vis Spectroscopy. ACS Catal. 2017, 7 (6), 4033–4046.
- (82) Xu, S.; Zhang, W.; Liu, X.; Han, X.; Bao, X. Enhanced In situ Continuous-Flow MAS NMR for Reaction Kinetics in the Nanocages. *J. Am. Chem. Soc.* **2009**, *131* (38), 13722–13727.
- (83) Hou, G.; Yan, S.; Trébosc, J.; Amoureux, J.-P.; Polenova, T. Broadband homonuclear correlation spectroscopy driven by combined R2nv sequences under fast magic angle spinning for NMR structural analysis of organic and biological solids. *J. Magn. Reson.* **2013**, 232, 18–30.
- (84) Frisch, M. J.; Trucks, G. W.; Schlegel, H. B.; Scuseria, G. E.; Robb, M. A.; Cheeseman, J. R.; Scalmani, G.; Barone, V.; Mennucci, B.; Petersson, G. A.; Nakatsuji, H.; Caricato, M.; Li, X.; Hratchian, H. P.; Izmaylov, A. F.; Bloino, J.; Zheng, G.; Sonnenberg, J. L.; Hada, M.; Ehara, M.; Toyota, K.; Fukuda, R.; Hasegawa, J.; Ishida, M.; Nakajima, T.; Honda, Y.; Kitao, O.; Naka, H.; Vreven, T.; Montgomery, J. A.; Peralta, J. E.; Ogliaro, F.; Bearpark, M.; Heyd, J. J.; Brothers, E.; Kudin, K. N.; Staroverov, V. N.; Kobayashi, R.; Normand, J.; Raghavachari, K.; Rendell, A.; Burant, J. C.; Iyengar, S. S.; Tomasi, J.; Cossi, M.; Rega, N.; Millam, J. M.; Klene, M.; Knox, J. E.; Cross, J. B.; Bakken, V.; Adamo, C.; Jaramillo, J.; Gomperts, R.; Stratmann, R. E.; Yazyev, O.; Austin, A. J.; Cammi, R.; Pomelli, C.; Ochterski, J. W.; Martin, R. L.; Morokuma, K.; Zakrzewski, V. G.; Voth, G. A.; Salvador, P.; Dannenberg, J. J.; Dapprich, S.; Daniels, A. D.; Farkas, O.; Foresman, J. B.; Ortiz, J. V.; Cioslowski, J.; Fox, D. J. Gaussian 09, rev. B.01; Gaussian, Inc.: Wallingford, CT, 2010.
- (85) Van der Mynsbrugge, J.; Moors, S. L. C.; De Wispelaere, K.; Van Speybroeck, V. Insight into the Formation and Reactivity of Framework-Bound Methoxide Species in H-ZSM-5 from Static and Dynamic Molecular Simulations. *ChemCatChem* **2014**, *6* (7), 1906–1918.
- (86) Chai, J.-D.; Head-Gordon, M. Long-range corrected hybrid density functionals with damped atom-atom dispersion corrections. *Phys. Chem. Chem. Phys.* **2008**, *10* (44), 6615–6620.
- (87) Kresse, G.; Furthmüller, J. Efficient iterative schemes for ab initio total-energy calculations using a plane-wave basis set. *Phys. Rev. B: Condens. Matter Mater. Phys.* **1996**, 54 (16), 11169–11186.
- (88) Perdew, J. P.; Burke, K.; Ernzerhof, M. Generalized Gradient Approximation Made Simple. *Phys. Rev. Lett.* **1996**, 77 (18), 3865–3868.
- (89) Hammer, B.; Hansen, L. B.; Nørskov, J. K. Improved adsorption energetics within density-functional theory using revised Perdew-Burke-Ernzerhof functionals. *Phys. Rev. B: Condens. Matter Mater. Phys.* 1999, 59 (11), 7413–7421.
- (90) Grimme, S.; Antony, J.; Ehrlich, S.; Krieg, H. A consistent and accurate ab initio parametrization of density functional dispersion correction (DFT-D) for the 94 elements H-Pu. *J. Chem. Phys.* **2010**, 132 (15), 154104.
- (91) Hutter, J.; Iannuzzi, M.; Schiffmann, F.; VandeVondele, J. cp2k: atomistic simulations of condensed matter systems. *WIREs Comput. Mol. Sci.* **2014**, *4* (1), 15–25.
- (92) Goedecker, S.; Teter, M.; Hutter, J. Separable dual-space Gaussian pseudopotentials. *Phys. Rev. B: Condens. Matter Mater. Phys.* **1996**, *54* (3), 1703–1710.

- (93) Laio, A.; Parrinello, M. Escaping free-energy minima. *Proc. Natl. Acad. Sci. U. S. A.* **2002**, 99 (20), 12562–12566.
- (94) Barducci, A.; Bonomi, M.; Parrinello, M. Metadynamics. Wiley Interdiscip. Rev.: Comput. Mol. Sci. 2011, 1 (5), 826–843.
- (95) De Wispelaere, K.; Wondergem, C. S.; Ensing, B.; Hemelsoet, K.; Meijer, E. J.; Weckhuysen, B. M.; Van Speybroeck, V.; Ruiz-Martinez, J. Insight into the Effect of Water on the Methanol-to-Olefins Conversion in H-SAPO-34 from Molecular Simulations and in Situ Microspectroscopy. ACS Catal. 2016, 6 (3), 1991–2002.
- (96) Marcos-Alcalde, I.; Setoain, J.; Mendieta-Moreno, J. I.; Mendieta, J.; Gómez-Puertas, P. MEPSA: minimum energy pathway analysis for energy landscapes. *Bioinformatics* **2015**, *31* (23), 3853–3855.